We are IntechOpen,
the world's leading publisher of
Open Access books
Built by scientists, for scientists

6,900
Open access books available

185,000
International authors and editors

200M
Downloads

154
Countries delivered to

Our authors are among the

TOP 1%
most cited scientists

12.2%
Contributors from top 500 universities

BOOK CITATION INDEX CLARIVATE ANALYTICS INDEXED

WEB OF SCIENCE™

Selection of our books indexed in the Book Citation Index
in Web of Science™ Core Collection (BKCI)

Interested in publishing with us?
Contact book.department@intechopen.com

Numbers displayed above are based on latest data collected.
For more information visit www.intechopen.com

Methods for Image Recognition of Charged Particle Tracks in Track Detector Data Automated Processing

A.B. Aleksandrov, N.G. Polukhina and N.I. Starkov
Lebedev Physical Institute, Russian Academy of Sciences,
Moscow,
Russia

1. Introduction

The completely automated measuring facility PAVICOM has been created at the Lebedev Physical Institute and is successfully used for processing the data of track detectors (nuclear emulsions, X-ray films, olivine crystals from meteorites, mylar, CR-309) (Aleksandrov et al., 2005a, 2005b, 2006, 2007a, 2007b, 2007c, 2010; Alexandrov et al., 2008; Belovitsky et al., 2006; Vladymyrov et al., 2008).

Track detectors have been widely used in particle physics experiments for many decades now. Such a long-standing life of the method is, certainly, due to the unique spatial resolution and the possibility of separating particle tracks.

The first track detectors were extremely simple: they were common photographic plates used by photographers at that time (early 20th century), as well as electroscopes. The Wilson cloud chamber makes use of the condensation of liquid from supersaturated vapour (under suitable conditions, ionization performed by a charged particle in a substance may cause a phase transition in it). The device was invented in 1912 by Charles T.R. Wilson (Wilson, 1897), who for many years had studied the physics of cloud formation in the atmosphere. The bubble chamber was invented and refined in early 1950s by D.A. Glaser (Glaser, 1952) (use is made of a superheated liquid, which boils near the nucleation centres – local energy-release sites ≥ 0.1 keV in the trajectory of a particle in the superheated liquid). Cloud chambers and bubble chambers make it possible to directly observe tracks of particles. This means that the position of a particle can be determined accurate to the size of a drop or a bubble, i.e., approximately up to 1 mm. However, the drawbacks of these thermodynamic chambers are their low-rate response, low spatial resolution and, above all, impossibility of automating data collection/processing on a real-time basis. These drawbacks were eliminated in detectors of another (electronic) type – gas-discharge counters with gas amplification, proportional and drift chambers, scintillation and Cherenkov detectors, solid-state detectors.

The simplicity of track detectors secures them a significant advantage over many other detection systems. The advantage of track detectors as integral instruments accumulating information under conditions of small fluxes of particles has been used not only in aerostat

experiments but also in satellite experiments with cosmic rays (Chan & Price, 1975). Track detectors (nuclear emulsions including) played an outstanding role in the development of nuclear physics due to their visual character and the possibility to obtain a comprehensive spatial pattern of processes studied. Nuclear decays and reactions, as well as novel particles (positron, muon, charged pions, strange and charmed particles) have been discovered owing to these detectors.

The track detection technique is also widely used in quite a number of applied works. Thus, data on the energy spectrum of reactor neutrons are obtained by means of neutron dosimeters containing dividing layers and track detectors (Burger et al., 1970). Using track detectors, information is obtained on the distribution of radiologically essential α-emitting natural nuclei of inert gases ^{222}Rn and ^{230}Rn (from, respectively, decays of ^{238}U and ^{232}Th), which, diffusing from a solid (a rock or a structural material) get into the atmosphere and may create a hazardous level of radiation (Fremlin & Abu-Jarad, 1980). Radon irradiation time in uranium mines is controlled by strips of cellulose nitrate fixed on miners' helmets (Frank & Benton, 1975). Registration of α-particles from radon gas has been used in attempts to predict earthquakes because an increase of seismic hazard before earthquakes is often noted to be accompanied by the emergence of cracks and stresses; herewith, a large amount of radon is released from uranium and thorium occurring in the Earth's crust (Savvides et al., 1985). The track detection method is also used in studies of the exchange processes in the troposphere, where radon is used as an indicator (Birot et al., 1970). Track detectors are used in beams of negative pions in radio therapy to study events with high linear losses of energy (Benton et al., 1970; Fowler & Perkins, 1961). Thus, the method of track detectors is constantly developing, its protocol is being refined, and at present there is hardly a field of science and technology where it is not used. These are high energy physics, cosmic ray physics, reactor physics, metallurgy, geology, archeology, medicine, biology, studies of meteorites and lunar samples (Benton et al., 1970; Birot et al., 1970; Burger et al., 1970; Chan & Price, 1975; Frank & Benton, 1975; Fowler & Perkins, 1961; Fowler et al., 1970; Fremlin & Abu-Jarad, 1980; O'Sullivan et al., 1980; Price et al., 1967, 1968; Savvides et al., 1985).

However, none of the elementary particle detectors currently used can provide for the spatial resolution given by nuclear emulsion: at a grain size of 0.3–1 µm, the deviation of grains from the recovered trajectory of a particle does not on average exceed 0.8 µm, and under certain conditions can be reduced to 0.2 µm. The use of a double-sided emulsion makes it possible to determine the particle-movement direction accurate to less than one milliradian. Nuclear emulsion is used in quite a number of experiments by physicists in Europe, America and Asia. The largest of them can contain tons of nuclear emulsion, which corresponds to thousands of square metres of emulsion surface (Acquafredda et al., 2009; Eskut et al., 2008; Kodama et al., 2008).

In this context, of paramount importance are methods, which should provide for a fast and high-quality retrieval of information from data obtained by means of track detectors. Browsing of large areas of detectors (as a rule, at high magnification) poses a rather complex technical problem. Manual examination of track detector data in optical microscopes by an operator required enormous input of labour and time. The measurement rate proved not high, which determined the low statistics of processed events. Besides, the probability of hard-to-find errors is sufficiently high in such measurements, so the obtained results poorly yielded to checks for possible failures occurring in the processing of material (e.g., losses of particle tracks by measurers and other errors).

In recent years, this drawback has been largely overcome owing to progress in production of precision instruments and the development of optical tables with high accuracy of computer-aided displacement, extensive use of modern CCD and CMOS video cameras for recording and digitizing optical images, and computing power of modern computers. Complete automation of microscopists' labour became a reality owing to the use of these achievements in precision mechanics, potential of computer means and development of required software. In such automatic measurements, digitized images of tracks of charged particles and nuclei in track detectors obtained by means of video cameras are entered into computers, whose software makes possible the search for, and recognition and examination of tracks, and enables the reconstruction of their spatial position. Such an automated method of measurements excludes almost totally the use of microscopist's wearisome visual work and accelerates processing by about three orders of magnitude as compared with the use of the so called semiautomatic devices. The new method makes it possible to process large arrays of experimental data and to significantly increase the statistics of events, which was earlier unrealistic in practice. The development of similar automated facilities is of current interest, as it enables transition to a higher level of experimentation making use of the track detector technique and significantly expands the sphere of problems, where it can be efficiently used.

PAVICOM-1   PAVICOM-2

PAVICOM-3

Fig. 1. Appearance of the three microscopes of the PAVICOM facility.

The development of automated facilities was pioneered by Japan, where such a facility has been created well back in mid 1980s. But the real impetus to the development of automated facilities throughout the world were CHORUS and DONUT experiments (Eskut et al., 2008;

Kodama et al., 2008), which made use of significant amounts of nuclear emulsion. At present, only the OPERA experiment employs hundreds of tons of nuclear emulsion, which corresponds to hundreds of thousands square metres of emulsion surface. About 40 automated facilities in total are operated at present throughout the world, 20 of which are in Europe, where in the recent years the number of such facilities rapidly increases.

2. Equipment of the PAVICOM facility

In Russia, there is only one facility of such a level, which satisfies modern international standards. This is the high-tech completely automated measuring facility PAVICOM. It is intended for processing the data of emulsion and solid-state track detectors used in various physical studies and satisfies the most modern world standards (Feinberg et al., 2004). Initially, the facility was developed to process materials of LPI's EMU-15 experiment (Astafyeva et al., 1997; Boos et al., 1996; Chernavskaya et al., 1996; Dobrotin et al., 1999; Dremin et al., 2001a), in which the emulsion chamber including a lead target 0.4 mm thick with the succeeding stack of 38 layers of nuclear emulsion was irradiated by a beam of lead nuclei with energy of 158 GeV/nucleon. However, the versatility and potentially high hardware potential of the PAVICOM facility provided for in the course of its development enabled its use for a significantly broader sphere of problems (Polukhina, 2006). Staff members of about 10 Russian and several foreign institutes together with LPI's PAVICOM group are involved in processing and analysis of experimental data.

PAVICOM consists of three independent completely automated installations, which differ, first and foremost, in the optical tables' displacements and, respectively, admissible sizes of the processing detectors (Fig. 1).

The main units of the PAVICOM-1 installation are the automatic precision table (MICOS, Germany); the optical system, which is set up in accordance with the problem solved; Pentium computer. The MICOS precision mechanical system consists of the massive metal platform and movable object table, whose displacement limits in the horizontal plane are 400 mm × 800 mm. The CCD camera fixed over the table can be moved vertically within the limits of 0 to 200 mm. The coordinates in all three axes are measured accurate to 0.5 μm. The optical table and vertical ruler are displaced by means of the step motors driven by the controller operated by the computer or (manually) by the joystick. The optical system of the microscope was created at the LPI using the components from LOMO (Russia). The microscope's optics project the image of an object on the CCD matrix of the VS-CTT system (Videoscan, Russia). The CCD pixel resolution is 1360 × 1024; colour depth, 10 bit. The installation is arranged in a clean room with glass walls.

The automated microscope PAVICOM-2 was created on the basis of the microscope MPE-11 (LOMO, Russia). The main units of PAVICOM-2 are the precision table (Carl Zeiss) with the control module; two digital CCD cameras; computer. The automatic displacement limits of the table along the X axis are 0–120 mm; along the Y axis, 0–100 mm; the vertical displacement limits are about 1 cm. The optical table is displaced along all the axes by step motors driven by a controller operated by computer. The coordinate measurement accuracy is 0.25 μm. The characteristics of the video equipment: (1) The pixel resolution of the first CCD camera is 768 × 576; colour depth, 8 bit. An image in the camera is produced by the objective lens of the microscope, with a magnification of up to 60×. An analog signal formed by the video camera is fed to the input of the analog-to-digital converter – the image capture and digitization board – which transfers the digitized signal to computer memory. (2) The

second video camera: CMOS MC1310 with 10-bit colour depth and pixel resolution of 1280 × 1024; shooting speed, up to 500 frames per second.

The third installation, PAVICOM-3, has the following main characteristics: the motorized movable table (MICOS); the microcontroller to operate the step motors (National Instruments); the illumination system (Nikon); the computer-controlled power supply unit for the illumination system, the computer, a dual-processor workstation based on Intel Pentium 4 Xeon 3.6 GHz; the video camera, CMOS MC1310 with 1024 grey levels, shooting speed up to 500 frames per second.

3. Principle of PAVICOM software construction

The PAVICOM facility makes use of two types of commercial image-digitization plates: VS-CTT and Matrox Odyssey XPro, using which an image is digitized and its primary processing is done. The entire subsequent image analysis is performed using specially developed software. The search for and digitization of the coordinates of charged particles' tracks in the material of the detector, computer-aided track recognition and tracing, data systematization and primary processing are done here in the completely automated mode. Mathematical processing of digitized images is performed by computer at a rate of up to 500 fps using a library of image processing programs written in C++. An image in the CMOS video camera is formed by the objective lens of the microscope. An analog signal formed by the video camera is fed to the input of the Matrox Odyssey XPro image, digitization and processing board.

The use of multiprocessor systems in automated scanning facilities enables a significant increase of their performance due to the simultaneous execution of various tasks. PAVICOM makes use of a dual-processor workstation based on Intel Xeon processors with Hyperthreading Technology support. The Matrox Odyssey image digitization and processing board is also a separate multiprocessor system. The complete use of PAVICOM's computing potential is possible only at the realization of an efficient multithreaded model in the software. Another way to increase the computing power of the system for solving labour-intensive computing tasks is to combine two or more computers into a common network. The computing load in this case is distributed between all computers of the network.

The modular approach to the construction of the software was used to implement all the requirements to its versatility and fast response. This approach makes it possible to incapsulate the implementation of the modules, i.e., none of the modules depends on the operation and design of the other modules. Correspondingly, a change in one module in no way affects the other modules. Thus, the required flexibility in the adjustment of the program is achieved, which enables it to perform scans on microscopes of various types. For this, it is only necessary to replace the software-dependent parts of the modules, the adaptors. The program can also be used for processing the data of various experiments. For this, the respective handler should only be implemented. Herewith, all the other modules of the program, not dependent on the hardware and the character of the experiment, would remain invariable at various variants of the adjustment.

4. Methods for image recognition of elementary particle tracks for EMU-15 experiment

In LPI's EMU-15 experiment performed at CERN, which made use of nuclear emulsion as a detector, the main aim was to search for possible signals of quark–gluon plasma formation

at ultrahigh temperatures and superdense states of matter. The experiment made use of 16 emulsion chambers shaped as cylinders 260 mm in length and 95 mm in diameter. Each chamber contained a thin (400 μm) lead target and 38 layers of nuclear emulsion (each 50 μm thick) poured on to a 25-μm thick mylar support. One layer of emulsion was positioned immediately before the target; the others were behind the target. The total thickness of each chamber was only 0.07 cascade lengths, which is extremely important at the registration of the central collisions of very high energy lead nuclei, in which thousands of secondary particles are generated. The chamber was placed into a transverse magnetic field of intensity 2 T and positioned such that the planes of the target and nuclear emulsions be perpendicular to the beam. The total number of Pb nuclei in irradiation of each of the 16 emulsion chambers was 10^4. About 10 central Pb–Pb interactions with multiplicity of secondary particles of more than 10^3 was found in each chamber (the criterion for selecting such events was the large multiplicity of secondary charged particles and the absence of fragments with charge $Z \geq 2$).

The image processing and microtrack search methods developed for this experiment enabled the first Russian automated search for tracks of secondary charged particles in central nucleus–nucleus interactions with multiplicity of >1500 in nuclear emulsion.

The automated processing of tracks in nuclear emulsion required the development of software to control the displacement of the microscope table, video shooting of images, their analysis and reconstruction of the geometric pattern of the projection of secondary charged particles.

The image processing task was divided into several stages:

- Preliminary search for and elimination of extraneous spots ("black" pixels of the video camera)
- Filtration of images
- Binarization of images
- Singling-out of connected regions (clusterization)
- Selection of clusters by size.

The result of image processing are sets of clusters assigned to one event.

The task of reconstructing the geometry of the projection of particles born as the result of nucleus–nucleus interaction was also split into several subtasks:

- Reconstruction of a microtrack (i.e., a segment of a microtrack in one of the emulsion layers) from a chain of clusters (tracking)
  - Calculation of the parameters of the microtrack by the given set of clusters (fitting)
  - Selection of clusters for the fitting without consideration of information on the interaction vertex (free tracking)
  - Search for the interaction vertex
  - Selection of clusters for the fitting with consideration of information on the interaction vertex (vertex tracking)
- Extension of the microtrack to the adjacent emulsion layer
  - Calculation of the track parameters by the given set of microtracks (linking)
  - Selection of microtracks for linking
- Determination of the direction of movement of the initial nucleus (search for the axis of the event).

The result of the reconstruction of particles' projection geometry after nucleus–nucleus interaction is a pseudorapid distribution of secondary particles, which is then analyzed in detail by various mathematical methods.

Images of particle tracks at the video camera output look like groups of blobs against the grey background (Fig. 2). Each pixel carries some information on the extent of image blackening (called colour). For the initial images the colour of a pixel is within the range of 0 to 255 (8 bit). For images converted by the filter the colour is described by a real number, and for binarized images by 0 or 1. At given depths of emulsion, 25 fields of vision were successively shot by the video camera by the spiral around the assumed centre of the event.
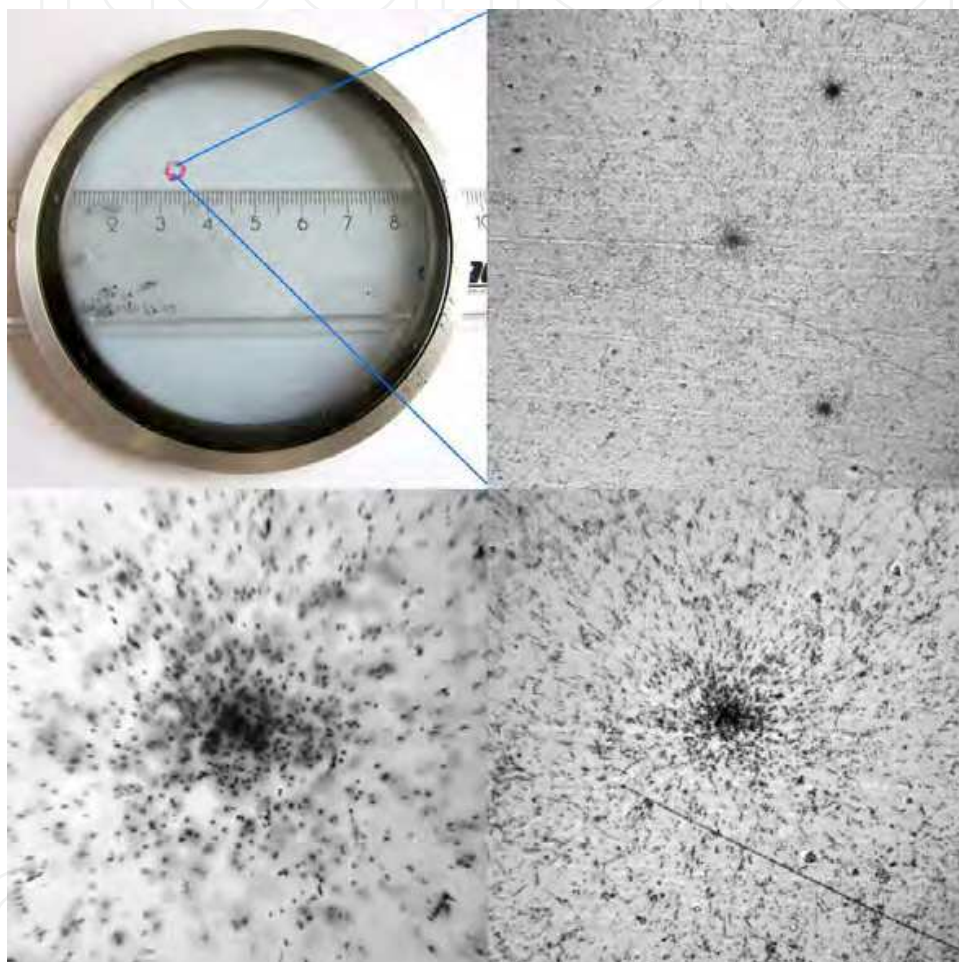
Fig. 2. *Top left*: an emulsion plate of EMU-15 experiment. *Top right*: the central field of vision at an objective-lens magnification of 8× (820 × 820 µm²). *Centre*, the tracks had not yet drifted apart and concentrate very densely, which makes the central region darker. Two tracks of noninteracting lead nuclei are also well seen on the image. *Bottom*: the same field of vision at a magnification of 20× (*right*, 330 × 330 µm²) and 60× (*left*, 115 × 115 µm²).

As nuclear emulsion was processed at a magnification, in practice it was impossible to completely rule out accidental specks (e.g., micron-size villuses on the video camera screen) in the field of vision, which led to the occurrence of dark spots on images (sets of "black" pixels) corresponding to background effects and undistinguishable from images of real blobs. They may hinder the correct reconstruction of microtracks or lead to the emergence of

false microtracks. (For instance, in Fig. 3 a Z-form speck is well seen at the right edge but two other specks are undistinguishable from the blobs.)

Preliminary search for such spots (sets of "black" pixels) is based on the fact that on all images they are at the same place. If on any image a "black" pixel has the coordinates (i, j), then on all the other images a pixel with the coordinates (i, j) shall be "black". Therefore, if the colours of pixels with the same coordinates are averaged by 25 images at the same depth, the defect regions should become more intensive: the colour of "black" pixels proves considerably more black than the colour of the other pixels (Fig. 3). Now the pixels assigned to defect regions can be removed by setting the same colour threshold for all fields of vision. Further on, the colours of the singled-out pixels are averaged by the neighbourhood of 20 × 20 pixels in size, after which they become practically undistinguishable from the background and, thereby, eliminated from the further processing (Fig. 4). Here and further, the background is meant to be the image background – the pixels not belonging to the images of blobs and, therefore, carrying no useful information.
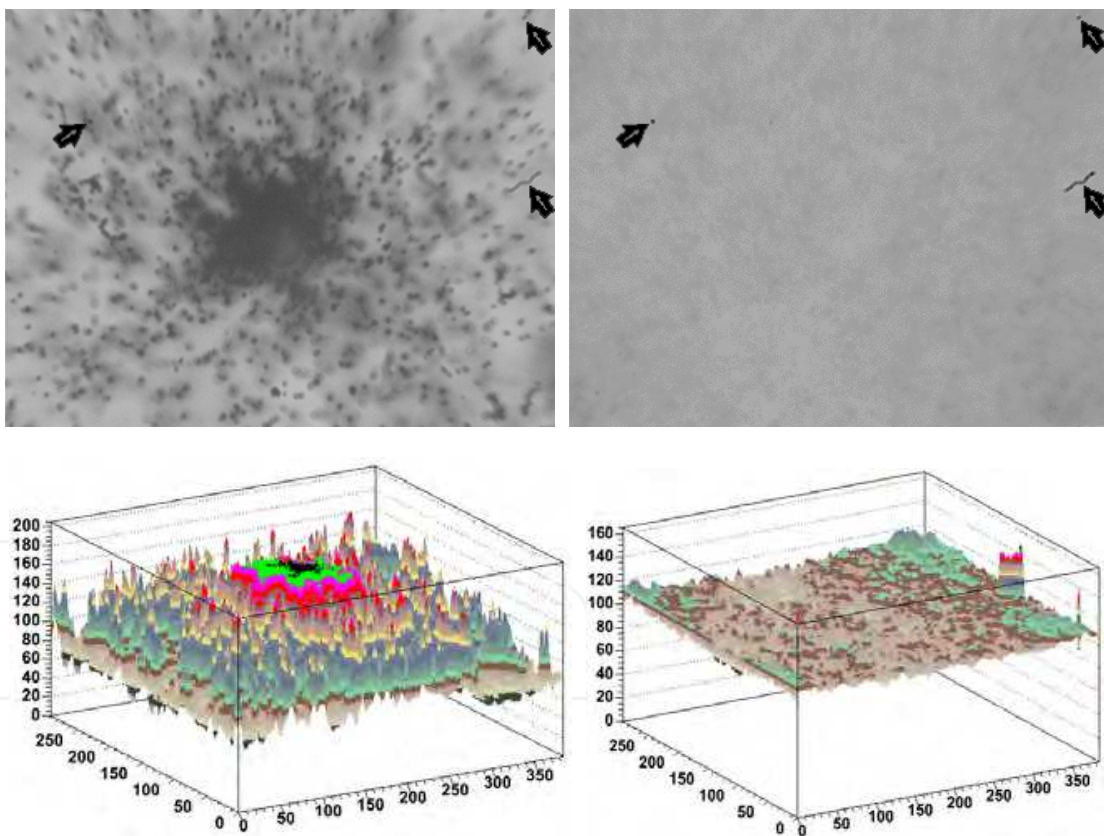

Fig. 3. *Top left*: initial image. Black arrows show spots formed from sets of "black" pixels. *Bottom left*: coordinate colour histogram of the initial image. *Top right*: image obtained as the result of averaging 25 images. *Bottom right*: its coordinate colour histogram. It is seen that in the case of the averaging the colours of "black" pixels do not change, which enables their easy finding by setting the pixel-colour threshold.
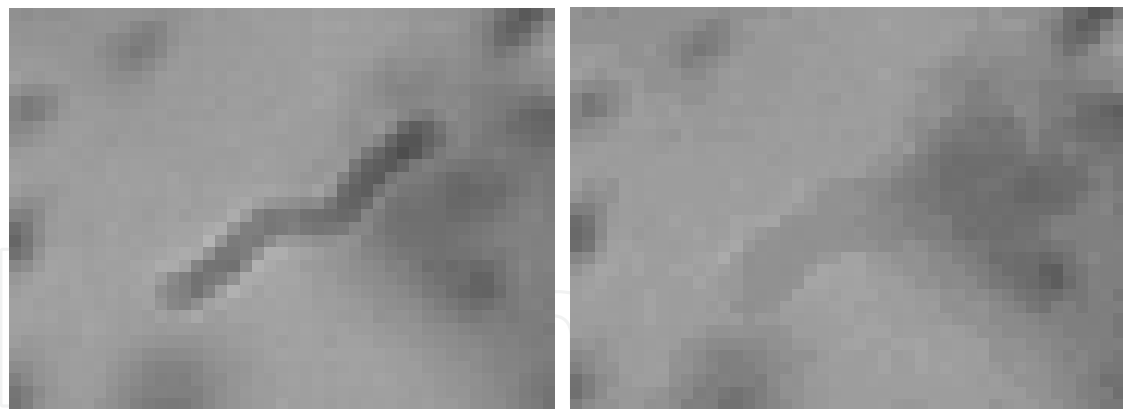
Fig. 4. Image of a Z-form speck before (left) and after (right) the removal of "black" pixels.

Filtration is the preliminary image-processing stage. Its aim is to single out spots which correspond to images of individual blobs. The expected intervals of sizes and extent of blackening of such spots are set beforehand.

To reduce the nonuniformity of the image background and to increase the quality of filtration in the darker central region of an image, the image is preliminarily processed. First, it is processed by a low-frequency averaging filter (Pratt, 1982). The filter blurs the images of separate blobs, owing to which the summary image becomes similar to the background, which would have been obtained in the absence of all blobs (Fig. 5).
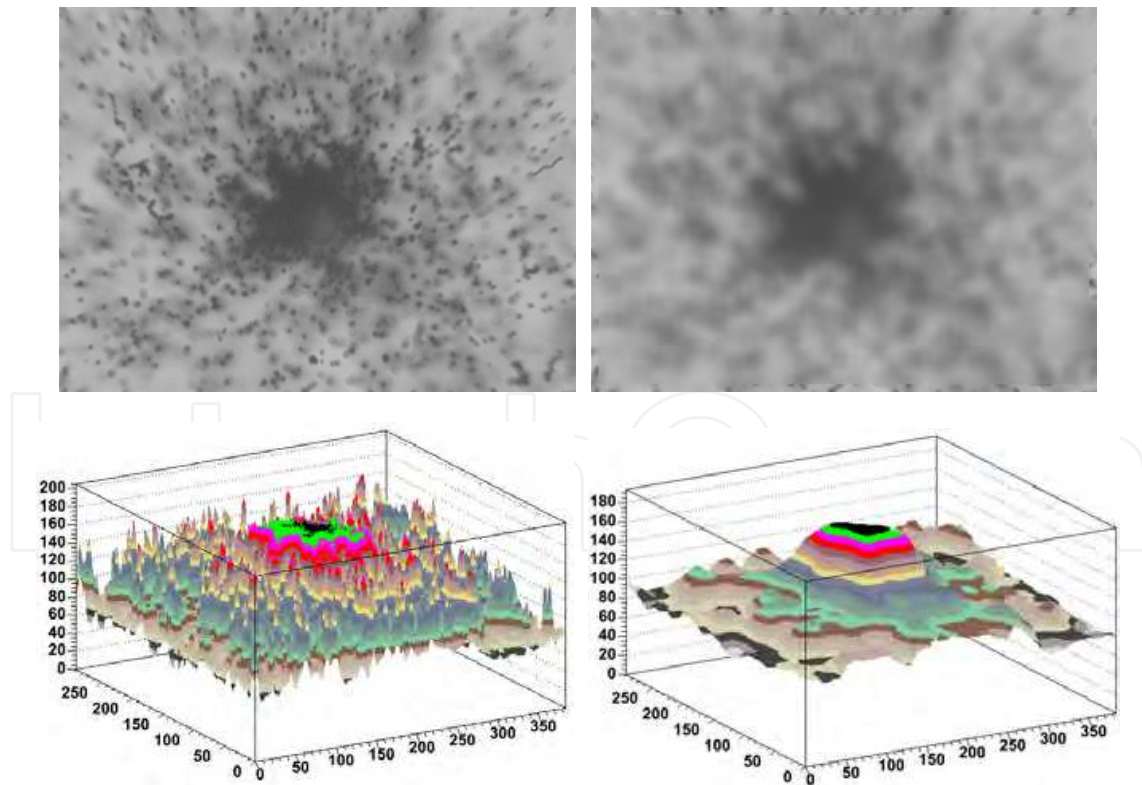
Fig. 5. *Top left*: initial image. *Bottom left*: coordinate colour histogram of the initial image. *Top right*: image processed by the averaging filter. *Bottom right*: its coordinate colour histogram. The filter blurs the images of all blobs to leave only the distribution of the darkening close to the background.

After this the pixel-colour conversion is done according to the formula:

$$c'_{i,j} = 255 \cdot (1 - \frac{c_{i,j}}{b_{i,j}}) \, ,$$

where $c_{i,j}$ is the pixel colour of the initial image and $b_{i,j}$ is the colour of the corresponding pixel of the averaged image. This procedure converts the pixel colours of the initial image into relative colours, thereby intensifying the images of the blobs in darker regions of the image (with lower $b_{i,j}$).

Subsequent filtration consists in the conversion of the image by the scanning high-frequency filter (Pratt, 1982), which reacts to the change of the extent of blackening on the edge of the spot. The size of the filter is chosen such that its response to spots similar to images of blobs forming the track of a particle were maximal. The result of this property of the filter is that the edges of blobs become more sharp, and blobs themselves more distinct, and their size and number do not change. Herewith, large spots formed by merged blobs (e.g., the large spot in the centre of Fig. 6) almost vanish after filtration, blending into the background of the image.
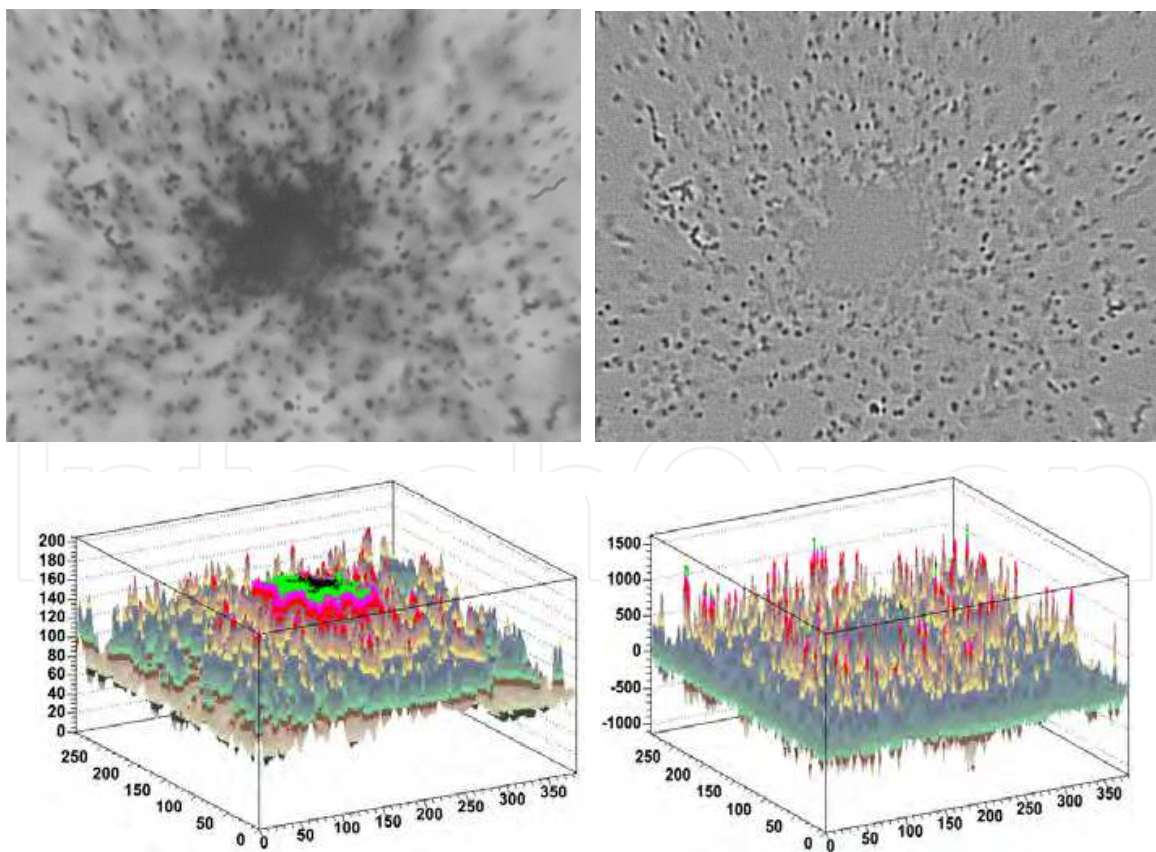

Fig. 6. *Top left*: initial image. *Bottom left*: coordinate colour histogram of the initial image. *Top right*: image processed by a high-frequency filter. *Bottom right*: its coordinate colour histogram. It is seen that the filter intensifies only spots of certain size and shape.

Mathematically, filtration is a matrix operation over pixel colours:

$$g_{i,j} = TrF^T C_{i,j},$$

where $g_{i,j}$ is the new pixel colour *(i,j)*, *F* is the filter matrix and $C_{i,j}$ is the matrix composed of the pixel colour *(i,j)* and the colours of the enclosing pixels such that the colour $g_{i,j}$ of the pixel *(i,j)* is the central element of the matrix $C_{i,j}$.

After filtration, the coordinate colour histogram of an image represents a multitude of narrow high peaks in those places where on the image there were characteristic spots – images of blobs. Comparison of the right- and left-hand parts of Fig. 6 shows the extent of blob intensification in this operation.

Then the procedures of binarization and clusterization were performed. Binarization is the process of singling-out the pixels, which correspond to the images of blobs (assigning colour 1 to these pixels). For this, a threshold restriction is imposed on an image: the pixels whose colour exceeds the threshold are assigned the value of 1, the others are assigned colour 0. Clusterization is the singling-out of connected regions – integration into clusters, which correspond to spots of blackening (blobs) in nuclear emulsion, of pixels with colour 1 singled out in the process of binarization. Knowing the coordinates (x_i, y_i) of each pixel in a cluster, we can find the centre of masses, the mean radius and the area of the cluster.
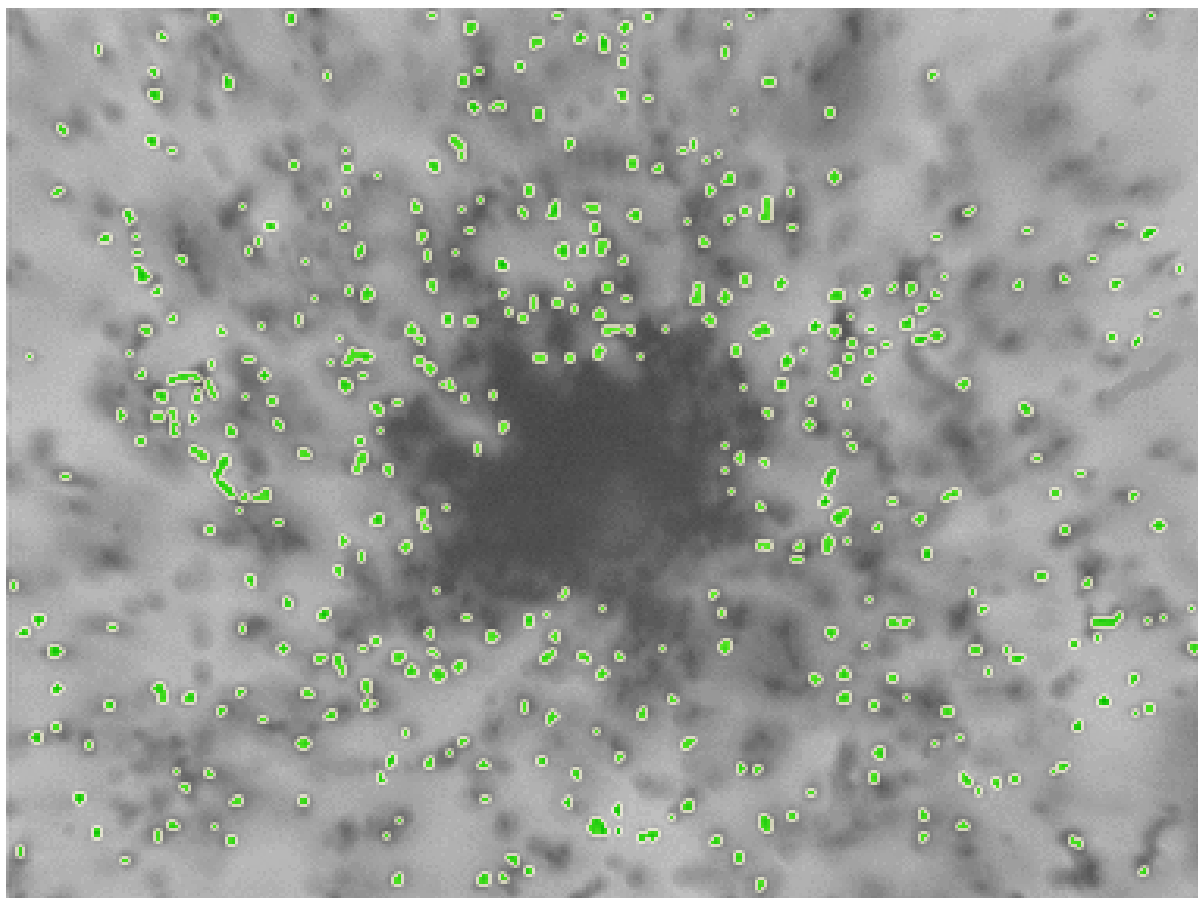

Fig. 7. The result of clusterization of the central field of vision. The clusters found are highlighted.

Thus, physical objects (blobs) are put in correspondence with mathematical objects (clusters). The results of clusterization of the central field of vision are given in Fig. 7.

Clusterization yields sets of points – centres of masses of clusters on the plane corresponding to a certain depth. By adding the results of the measurements along the Z axis (i.e., along the depth of the fields of vision), we obtain sets of clusters distributed in the volume studied. Further, it is necessary to reconstruct the microtrack of a particle from the sets of clusters. (The microtrack is part of the track of a particle, which part lies inside a particular layer of emulsion.) For this purpose, the microtrack is depicted by a straight line given by a point with the coordinates *(x, y, z)* and slopes (*tx, ty*) of the projections of this line on the plane *XZ* and *YZ* to the axis. The Z axis is perpendicular to the plane of emulsion and is codirected to the beam of particles. The coordinate origin along the Z axis is chosen on the front plane (relative to the beam) of the target. Reconstruction of the microtrack by the given set of clusters (drawing the straight line through the known set of coordinates of the centres of mass of the clusters – the fitting) was done by the method of least squares (Bock et al., 2000). When selecting the clusters for microtrack recognition (the so called "tracking"), several requirements were to be satisfied: at each depth inside emulsion (i.e., on the plane of the clusters), no more than one cluster is assigned to a track; the distance between two successive clusters should not exceed a given value; the number of clusters in a microtrack should be no less than the preset value.

Due to a large number of clusters, it does not appear to be possible to consider all combinations of their chains in full measure over reasonable time. Therefore, the search for tracks is done in several stages: free tracking, search of the interaction vertex and vertex tracking.

The algorithm of the free tracking is illustrated in Fig. 8. An arbitrary cluster (x^0_i, y^0_i) on the emulsion plane z^0 nearest to the target is considered. The perpendicular (tx_0, ty_0) is taken as the initial direction, and a cone with the vertex at (x^0_i, y^0_i, z^0_i) and preset angles (s^0_x, s^0_y) in the *XZ* and *YZ* planes between the generatrices and the axis (tx_0, ty_0) is constructed around it. Around the selected cluster a sphere is constructed, which *a fortiori* captures several depths, and clusters getting into this sphere are picked out. By these clusters, all possible combinations of microtracks in the cone are made up (set *C*). Successively adding clusters one by one from *C*, we construct a set of chains of clusters, which is sorted out by the criterion χ^2.

This procedure is performed for each chain of clusters. Herewith, the direction of the microtrack, which corresponds to a chain, is taken to be the axis of the cone, and the vertex of the cone is constructed at the point of intersection of this microtrack with the plane corresponding to the Z coordinate of the last cluster in the chain.

As the result, we obtain a set of microtracks (chains of clusters), which originate from one common cluster (x^0_i, y^0_i). Then we choose a track with the lowest χ^2 and with the number of clusters not smaller than that given for the chain corresponding to it. The constituent clusters of the microtrack are marked as used and are not involved in further tracking. The same procedure applies to all clusters on the next planes, so that the origin of the microtrack can be at any depth along Z. The tracking is stopped if all layers are passed or if no candidates are available in several layers.
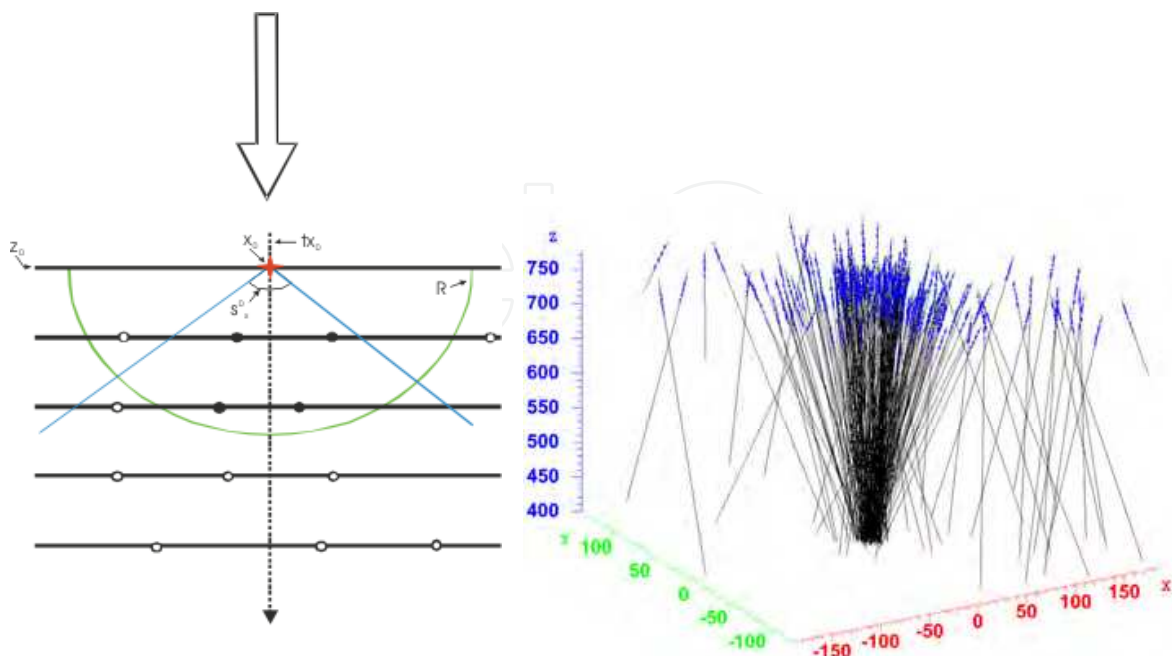
Fig. 8. *Left*: an illustration of free tracking (see text). Solid horizontal lines correspond to various depths of emulsion. The Z axis is directed downwards and is codirected with the beam of particles (arrow). The vertex of the cone is in the current cluster. The direction around which the cone is constructed is shown by a dashed line. Clusters, which got into the cone and the distance to which from the vertex does not exceed R (marked with black circles) will be used in building-up the track, the other clusters (white circles) are ignored. *Right*: the result of free tracking. It is seen that most particles escape from the common centre with $z \sim 400$ μm.

As the result of this procedure, we have a set of microtracks as shown in Fig. 8.

In the search for the interaction vertex, all found microtracks are initially the components of microtrack set A. To find the initial values of the vertex coordinates, for each pair of microtracks from set A we searched for pairs of points of closest approach (set B). Then an average value μ of the coordinates of all points from B is found.

For each track from set A, a point of closest approach with μ is found (set C), and the coordinate distributions of such points are constructed. From these distributions, the new values of μ and their root-mean-square errors σ_μ are determined. From set A, microtracks are excluded for which the points of closest approach with μ lie at distances exceeding $3\sigma_\mu$. The procedure is repeated until all microtracks from A are within $3\sigma_\mu$, i.e., when none of the microtracks could not be excluded from A. An elliptic cylinder with the sizes of the axes of the ellipsis along X and Y, depending on the measuring errors, and the height Z equal to the thickness of the target, is considered to be the region of the vertex.

The final stage of microtrack recognition – the vertex tracking – takes into consideration that the EMU-15 experiment investigates central collisions. In this case, the projection of all tracks of one event to the plane perpendicular to the beam has a pronounced centre with the coordinates (x^c, y^c).
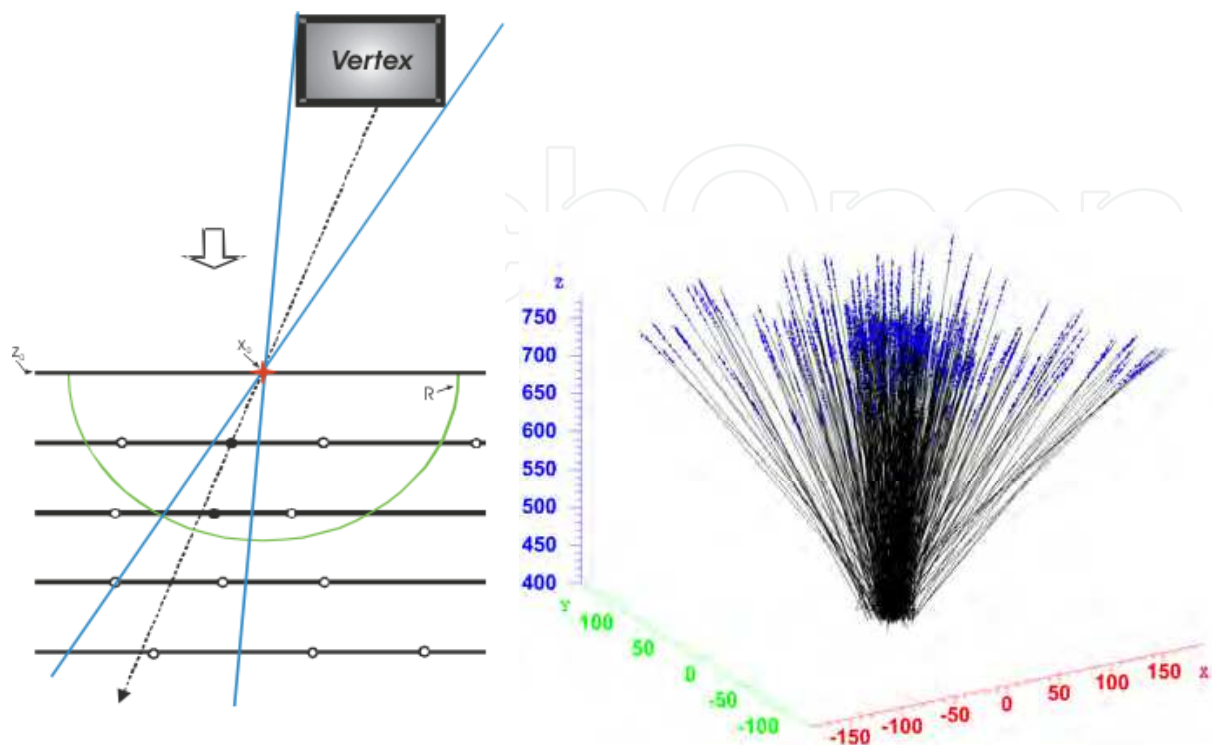
Fig. 9. *Left*: an illustration of vertex tracking. Solid horizontal lines correspond to various depths of emulsion. The Z axis is directed downwards and is codirected with the beam (arrow). The vertex of the cone is in the current cluster. The direction around which the cone is constructed is shown by a dashed line. The clusters which got into the cone and the distance to which does not exceed R (shown by black circles) are used in building up the track. The other clusters (white circles) are ignored. *Right*: the result of vertex tracking.

The algorithm sets up a cylinder whose axis is parallel to the Z axis and passes through point $(x^c, y^c, 0)$. From above and from below the cylinder is limited by the planes perpendicular to the Z axis ($Z = z^c_1$ and $Z = z^c_2$) (Fig. 9). Further, an arbitrary cluster (x^0_i, y^0_i) on the upper plane of emulsion, $Z = z^0$, is selected. From the lower layers, clusters (set C) are picked out, for which the straight line connecting any cluster from C with the cluster (x^0_i, y^0_i) passes through the preset cylinder. By successively adding clusters one by one from C, a set of chains of clusters is constructed. The fitting of each chain is performed, and the obtained set of microtracks is sorted out with respect to χ^2. The described procedure is repeated for each chain of clusters. As the result, a set of microtracks (chains of clusters) is obtained, which originate from one common cluster (x^0_i, y^0_i). Then, microtracks with the lowest value of χ^2 and the limited number of clusters in the respective chain are successively selected. The clusters that form a microtrack are not involved in the further tracking. Then the procedure is repeated for the next layer.

The efficiency of tracking was checked in two ways: manually and by modelling the events of passing a charged particle through emulsion. The efficiency of microtrack recognition was 90% (for the central field of vision with high particle density) and 99% (for the other regions).
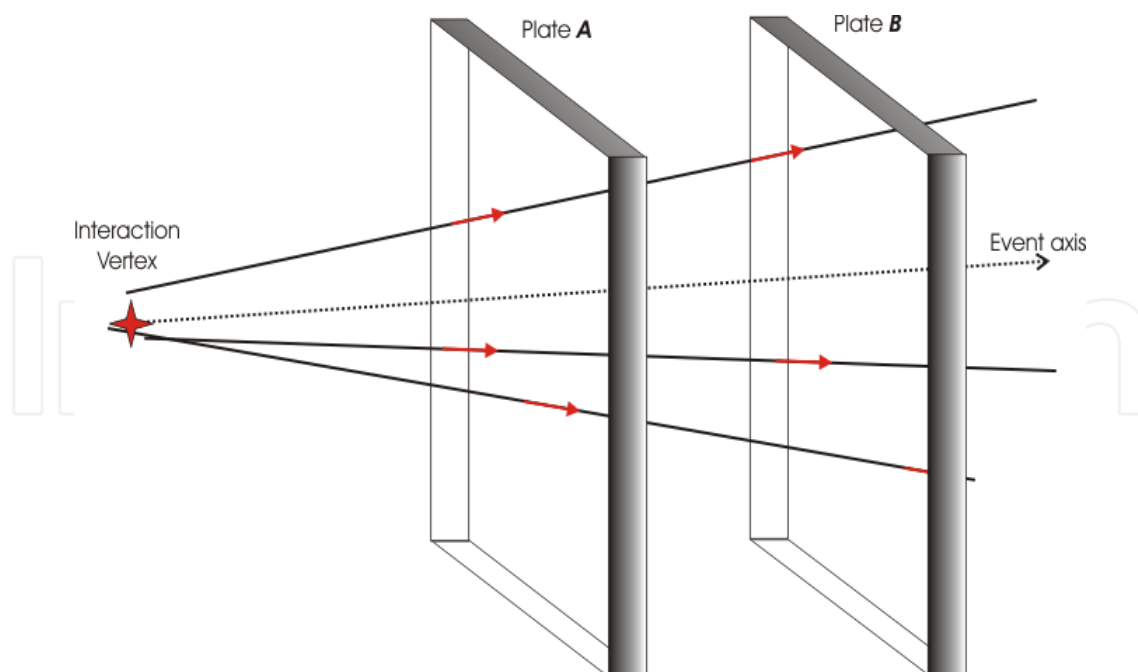
Fig. 10. Extension of microtracks to an adjacent layer of emulsion.

For microtrack linking, it is necessary to calculate the parameters of a track, which fits a given set of microtracks the best. This task is solved by the least squares method and is largely similar to the fitting task, see (Aleksandrov, 2009).

Finally, to determine the angular characteristics (pseudorapidity) of secondary particles formed in nuclear interaction, microtracks from adjacent emulsion layers are linked (Fig. 10). At the initial stage of this procedure, each microtrack from emulsion layer A is linked with each microtrack from adjacent layer B. Of all the diversity of variants, a track with minimal χ^2, passing through the interaction vertex, is chosen. As the result, a set of tracks (the so called target diagram), which consist of two parts and have a lower angular uncertainty than each particular microtrack, is obtained (Fig. 11).

For the search of the axis of an event, it should be taken into account that the direction of travel of the initial accelerated Pb nucleus can differ from the normal to the plane of the event owing to the divergence of the beam. At the same time, the axis of the event is given by the direction of travel of the initial nucleus. The algorithm of the search for the axis of an event is largely similar to the algorithm of the search for the interaction vertex. Based on the data on its coordinates x_c, y_c, the set of points of the maximal approach of tracks from set A with vertex c is constructed. From the initial set of tracks A, we exclude all tracks whose points of the maximal approach with vertex c are beyond $3\sigma_c$, where σ_c is the standard error of determining the position of point c. The angles of the remaining tracks with the axis of the event are averaged, and the initial direction of the axis is found. Then histograms of the angular distribution of tracks relative to this axis are plotted (Fig. 12), from which the new values of the direction of the axis are found. From A, we exclude tracks the angle between the direction of which and the direction of the axis exceeds $3\sigma_t$, where σ_t is the angle determination error. Then again histograms of angular distributions are plotted, and the procedure is repeated until the angles between the directions of all tracks prove to be inside $3\sigma_t$, i.e., when none of the tracks could be excluded from A.
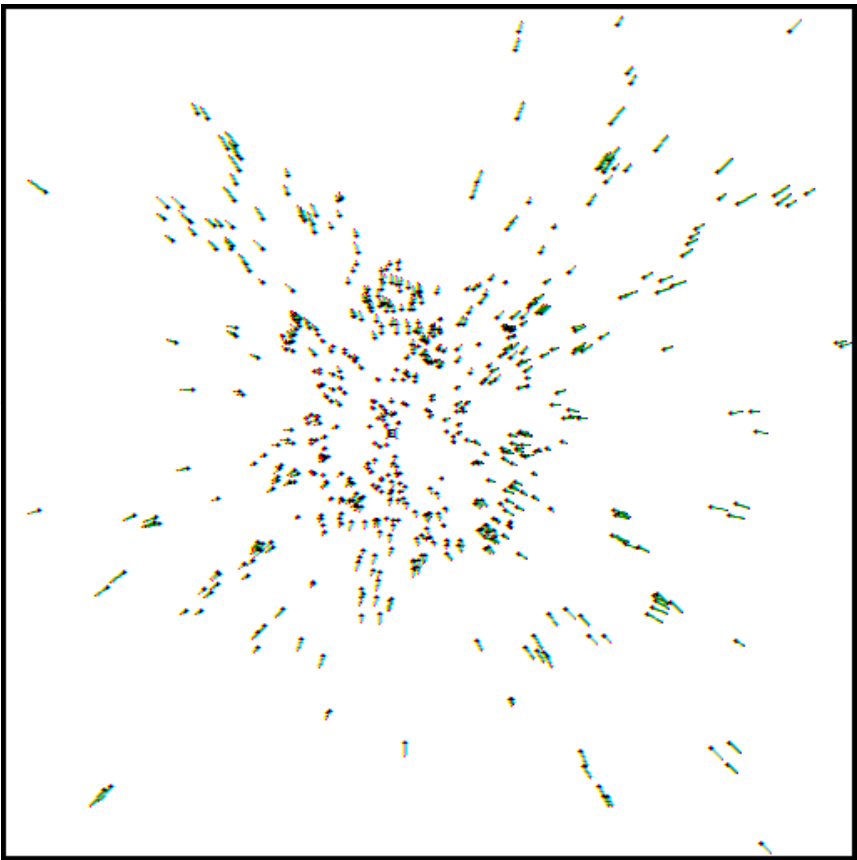
Fig. 11. The result of tracking and linking of two emulsion layers: a target diagram for 647 particles (event 5c15e).
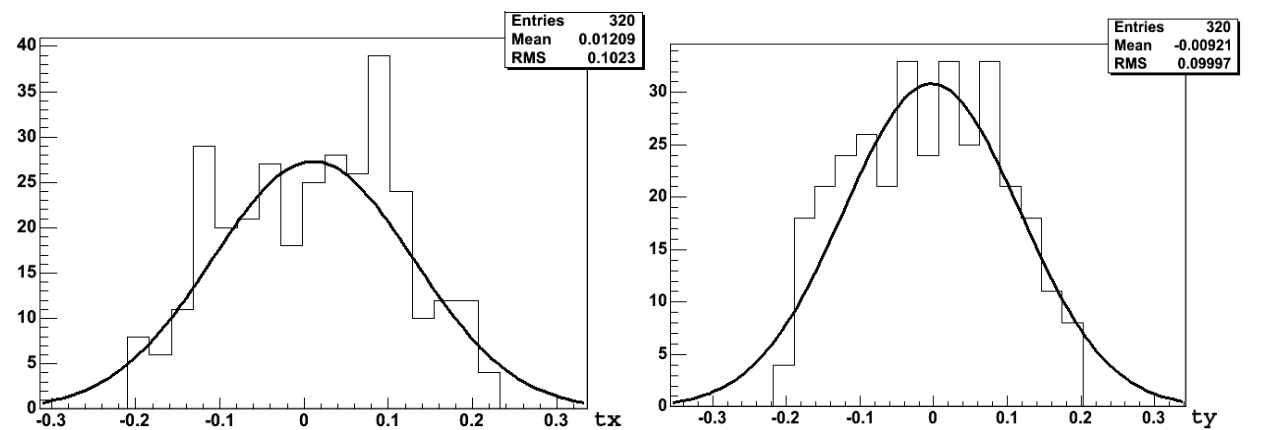

Fig. 12. An example of angular distributions of tracks relative to the axis of an event (*left*, *tx*; *right*, *ty*).

The procedure described was implemented as a library of programs (Aleksandrov, 2009). The first program, which includes algorithms of filtration, binarization, clustering, search for the interaction vertex, free and vertex tracking was implemented as the image handler for the automation program. This enabled the processing of images, search for clusters, interaction vertex and microtracks in real time mode over a time of less than 1 min. The algorithms of linking, search for the axis of an event and physical analysis were implemented in a separate program. Both programs were implemented using C++.

Thus, in accordance with the algorithm of the image processing program for EMU-15 experiment, we successively carried out discrimination of "black" (background) pixels, filtration of images, binarization of images, isolation of connected regions (clusterization), filtration of clusters. All stages of the program were thoroughly checked, for which the real interaction was methodically filmed with a step of ¼ micron by depth. A practically total correspondence of the program-operation results to the characteristics of real emulsion confirms the correctness of the developed and executed algorithm of clusterization.

The performance of the tracking software package was checked by visual measurements and on model interactions. The efficiency of charged-particle track reconstruction was greater than 90%. The experimental data obtained in this way make it possible to study the peculiarities of the angular distributions of particles, to search for multi-particle correlations, the emergence of which can be expected in hadronization of excited nuclear matter, and to analyse these distributions with the view of searching for signals specific for quark–gluon plasma. The processing results were demonstrated using event 5c15e as an example (Fig. 13); a databank was created and a preliminary processing of 100 events was done.

The successfully solved image recognition problem made it possible to find microtracks in nuclear emulsion with high efficiency. Herewith, original image-processing algorithms were developed: filtration, binarization and clusterization (search for images of metal silver grains in nuclear emulsion). A detailed study of individual interactions can help find new rare phenomena, and conclusions obtained therewith will be statistically significant owing to a large number of particles born in an individual event: a large number of secondary particles are born in collisions of high-energy nuclei in EMU-15 experiment. Analysis of their distribution in phase space is the main aim of the study, as it enables conclusions on the dynamics of the process. This is not an easy task even if only particles' escape angles (polar and azimuthal) are measured, because the number of secondary particles sometimes exceeds 1000. The task is reduced to the recognition of images generated on the plane of the target diagram by this number of points. Wavelet analysis made it possible to solve this problem. Daubechies wavelet was first used in the processing of EMU-15 data for two-dimensional wavelet analysis of particle spectra. The result of this analysis was demonstrated by the example of studying the internal structure of the escape of secondary generated particles locally and on various scales. It was shown that on the distribution of secondary charged particles by pseudorapidity the correlated groups tended to be arranged as a ring around the centre of the diagram. This corresponds to groupings of particles at a constant polar angle, i.e., fixed pseudorapidity. The mechanism of the emergence of these structures in strong interactions can be explained by either an analog of Cherenkov radiation (gluons are discussed as an analog of photons), or else by the emergence of Mach waves (Dremin, 2006; Dremin et al., 2000, 2001b). Both discussed mechanisms have a similar nature – the emergence of radiation in the motion of a body in a medium at a velocity exceeding the phase velocity of the propagation of a disturbance in this medium.

The most significant indication of the existence of ring structures is the occurrence of two peaks in the pseudorapidity distribution (Fig. 13). Herewith, ring structures are seen on the plane of the target diagram (Fig. 14).

Thus, the processing of EMU-15 data taken as an example confirmed the nonsymmetric character of the distribution of secondary charged particles by the azimuthal angle in combination with pseudorapidity peaks in an individual event. This is indicative of the
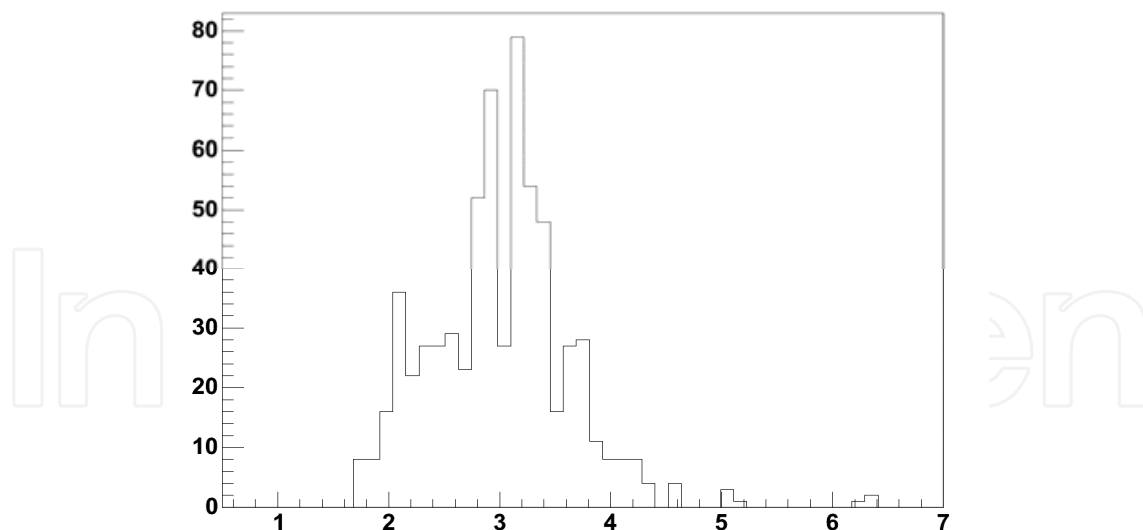
Fig. 13. Distribution of pseudorapidities of secondary charged particles in event 5c15e after automated processing.

peculiar features of the escape, caused by multiparticle correlations, the emergence of which, in particular, was expected at a comparatively small number of emitted Cherenkov gluons in each ring.

5. Study of the characteristics of galactic cosmic ray nuclei in automated recognition of tracks in olivine crystals from meteorites

Processing of EMU-15 data is only one of the projects implemented at PAVICOM. The multipurpose unique measuring facility PAVICOM is successfully used for high-technology processing of experimental data in nuclear physics, cosmic ray physics, high energy physics obtained in studies with emulsion and solid state detectors. The facility is used to solve problems associated with high-speed information support of the analysis of intravolume and surface defects of the crystal lattice and the rupture of materials on the nanostructural level. Its main distinction from other similar systems in the world and an advantage is versatility – the automated installations of the facility process data obtained using both nuclear emulsions and plastic detectors, and also crystals of olivines from meteorites. The use of this automated facility makes it possible to process large arrays of experimental data and significantly increase the statistics of events, which had been practically unrealistic earlier. A broad range of topical problems of modern nuclear physics is being covered.

In particular, in 2006 the project OLIMPIYA (Russian acronym for **OLI**viny iz **M**eteoritov: **P**oisk Tyazhelykh **I** Sverkhtyazhelykh **YA**der = Olivines from Meteorites: Search for Heavy and Superheavy Nuclei) was started to be implemented at PAVICOM. Its task are studies of heavy and superheavy nuclei in cosmic rays and search for trans-Fermi nuclei with charges $Z \geq 110$ in crystals of olivines from pallasites. The issue of the existence of superheavy nuclei is of greatest significance for understanding the properties of nuclear matter. First and foremost, of interest is to verify the prediction (Strutinsky, 1967) of a significant increase in the stability of nuclei near the magic numbers $Z = 114$ and $N = 184$ (N, the number of neutrons), which could lead to the existence of "stability islands" of superheavy nuclei in this region. Confirmations of this prediction have been obtained in experiments under the direction of Yu.Ts. Oganesyan at a JINR accelerator, where recently the nuclei of elements
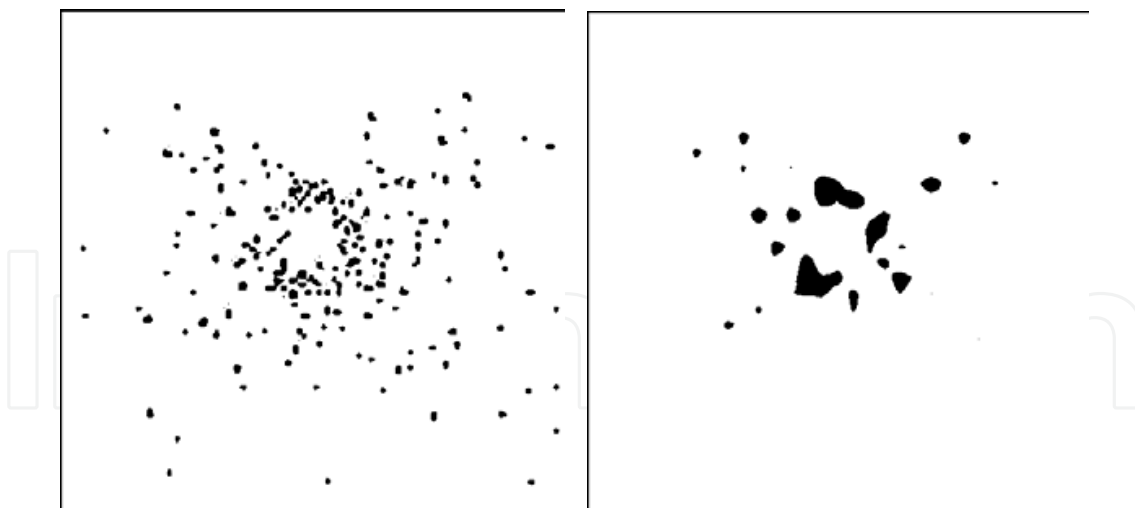
Fig. 14. Target diagrams of event 5c15e after, respectively, two and four iterations of inverse wavelet transformation.

114 and 116 have been discovered (Oganesyan, 2001) and the discovery of element 117 has been declared. The lifetimes of some of these nuclei are several seconds and even minutes, which exceeds tens of thousand times the lifetimes of nuclei with smaller charge.

According to the existing views, elements starting from carbon and heavier are formed in stellar interiors and at supernova explosions (Ginzburg, 1999). Heavy and superheavy elements being in Mendeleev's Periodic Table after bismuth are formed as the result of r (rapid) processes, which occur at a high concentration of neutrons and can lead to the formation of superheavy nuclei with the number of neutrons up to $N = 184$. Besides these traditional mechanisms, the possibility of the formation of very heavy nuclei (with the mass number of up to 500) at a high density of neutrons (of the order of 10^{30} cm^{-3}) and moderate temperature $T < 10^8$ K is discussed (Zeldovich, 1960). This situation can be realized in unequilibrium shells of neutron stars, ejections from which will lead to the emergence of super heavy elements in interstellar medium, stars and planets (Bisnovatyi-Kogan & Chechetkin, 1979; Kramarovsky & Chechev, 1987).

Measurements of the fluxes and spectra of heavy and superheavy nuclei in cosmic rays are an efficient way to study the composition of cosmic ray sources, processes occurring both in the sources themselves and in interstellar medium, in which cosmic rays propagate, and models of cosmic ray retention in the galaxy. The currently available experimental data on the abundance of heavy nuclei (with $Z > 50$) in the Universe, as well as on the spectra and fluxes of these nuclei in cosmic rays, are rather scarce, and for trans-Fermi nuclei no sufficiently reliable data are available at all. In the same way, there are no data on the possible existence of exotic superheavy nuclei, either.

The use of the factor of long-time exposure of meteorites in space leads to a great advantage of the method for the search of superheavy elements in crystals of olivine from meteorites as compared with methods based on the use of various satellite and aerostat detectors. The search for relict tracks left by particles of cosmic rays in meteorite minerals makes use of the ability of silicate crystals in meteorites (olivines, pyroxenes) to register and preserve for a long time ($>10^8$ years) tracks of nuclei with $Z > 20$. A typical age of meteorites and, therefore, their exposure time in the flux of cosmic rays is assessed to be 10^7–10^9 years. For

this reason, they may contain a large number of tracks of cosmic nuclei. As estimates show, 10^2–10^3 tracks of nuclei with $Z > 90$ can be formed over 10^8 years in 1 cm^3 of such crystals located at a depth of <5 cm from the preatmospheric meteorite surface, and up to 10^4 tracks in crystals from meteorite's surface layers (depth, < 1 cm). By measuring the track parameters, it is possible not only to identify particles but also to determine their energy spectra. Pallasite meteorites consist of iron–nickel "matrix", with inclusions of crystals of olivine – a yellow-colour semitransparent mineral up to 1–2 cm in size. As the previous works with olivines, the project OLIMPIYA is based on the used of the method of solid-state track detectors, in which particles are registered by the radiation damage they cause in the bulk of the detector material. A specific feature of the authors' method of the treatment of olivines from meteorites is the necessity of grinding, i.e., the irreversible disintegration of part of the crystal. Within the framework of the project OLIMPIYA, based on the PAVICOM facility, the technique for the recognition of tracks of nuclei in olivines was developed, the technique of scanning the entire area of the crystal, as well as the database of images to preserve information on tracks in the crystal.

Above we described in detail, using the processing of EMU-15 data as an example, the main stages of discrimination of tracks of particles as independent objects on individual images. The same methods were also used in studies of the characteristics of tracks of nuclei in olivines. First of all, coordinates of all pixels of each track should be obtained in particle track recognition. Then, based on this information, the characteristics of tracks are determined in accordance with the space of features chosen for this task. This procedure is performed in several stages.

First, depending on the quality of an image, a preliminary processing is carried out. Its aim is to maximally differentiate by the gradation of blackening the pixels of noise and the pixels belonging to tracks of particles, and to increase the efficiency of the binarization procedure.

The purpose of binarization is to separate analyzed objects from the background and noise. The discrimination of a subset on an image is equivalent to the setting of its "characteristic function", i.e., the function equal to unity in points of the subset and to zero in the other points. The generally recognized method of discrimination of some subset on the initial image is reduced to finding its characteristic function by quantification of the initial image to two levels. This procedure consists in determining the threshold of blackenings. All pixels with the blackening above the threshold are considered to belong to tracks of particles and are marked by black colour on the image. The other pixels are assigned to the background and noise and are marked with white colour.

The last stage of processing consists in discrimination of selected clusters (tracks) as independent objects (acquisition of the coordinates of pixels), determination of their characteristics and elimination of some of the remaining noise.

The set of transformations required at the stage of preliminary processing depends on the aims of this task, the quality of respective images and feature space. The preliminary processing results are present in several classes (in terms of C++), the volume of information in which can be chosen depending on the task and feature space. For this purpose, in the software developed for the project OLIMPIYA the classes for the description of clusters are constructed by the hierarchical principle. The main class Cluster0 containing minimal information about a cluster includes the number of pixels (cluster area) and their

coordinates (*X*, *Y*, *Z*) with indication of the cluster boundary. The derivative classes Cluster1, Cluster2 etc. contain additional information. Selection of a class to be used in a particular task depends on the requirements of the subsequent processing. Information about all clusters is gathered up in class Clusters, which also contains the functions of images' and particular clusters' processing. Due to distinctions in tracks of particles, the feature space can strongly differ for different tasks. Correspondingly, track images are processed differently in different experiments (Starkov, 2010).

The characteristics of clusters play an important role in the analysis of images. We adduce here techniques for determining the major of them.

Cluster area is simply equal to the number of pixels of which it consists, and is determined at the stage of cluster discrimination. A set of special algorithms was developed in the software package to obtain the other characteristics.

Each cluster is processed separately. First, the maximal and minimal coordinates *x* and *y* limiting the cluster are determined (see Fig. 15; it should be taken into account that in computer graphics it is accepted to direct the Y axis from top downwards). This cluster-limiting rectangle is required to assess the extent of its oblongness. Further, the *coordinates of the centre of masses* of the cluster pixels are calculated; they are its most important characteristic, which determines the position in space.

To find the *direction of axis of a cluster*, the coordinates of the midpoints of its lines are first determined. Further, using the least squares method, the obtained set of points is approximated by a segment of the straight line passing through the centre of masses (Fig. 15). This straight line is considered to be the axis of the cluster. Sometimes this procedure has to be repeated for the midpoints of the columns. This is due to the fact that at the first stage we can obtain not a longitudinal axis but a transverse axis. Then at the second stage the axis will for certain be longitudinal. An important characteristic of the axis is its slope. (For instance, in the problem of the scattering of neutron-excess nuclei (Starkov, 2010) it determines the direction of the search for the extension of the tracks of particles scattered at a large angle.)
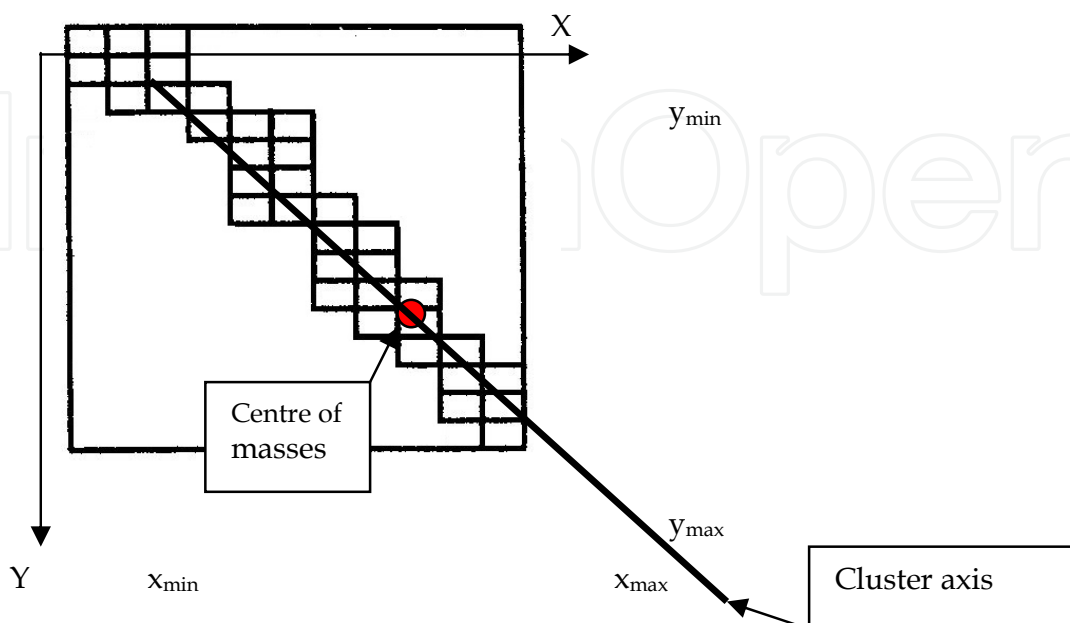

Fig. 15. Determination of the coordinates of a cluster.

There is a possibility to find the position of the axis and its directions by minimizing the momenta of inertia of the pixels relative to the straight line passing through the centre of masses of the cluster:

$$S_x = \sum x_i \qquad M_x = S_{xx} - \frac{S_x^2}{Area}$$

$$S_y = \sum y_i \qquad M_y = S_{yy} - \frac{S_y^2}{Area}$$

$$S_{xx} = \sum x_i^2 \qquad M_{xy} = S_{xy} - \frac{S_x \cdot S_y}{Area}$$

$$S_{yy} = \sum y_i^2$$

$$S_{xy} = \sum x_i y_i \qquad \Theta = \tan^{-1}\left\{ \frac{M_{xx} - M_{yy} + \sqrt{(M_{xx} - M_{yy})^2 + 4 \cdot M_{xy}^2}}{2 \cdot M_{xy}} \right\}$$

The *width of the cluster* is determined as a doubled mean distance of the pixels of the boundary to its axis. The *length* is determined as the length of part of the axis lying inside the cluster.

The above given definitions for the axis, width and length are sufficiently exact for clusters of convex or close to convex shape. If clusters are bent or have a more complex shape, these concepts cease to be exact and are not used. The shape of a cluster in this case is reflected more accurately, e.g., by the ratio of its area to a circle of a diameter equal to the length of the cluster.
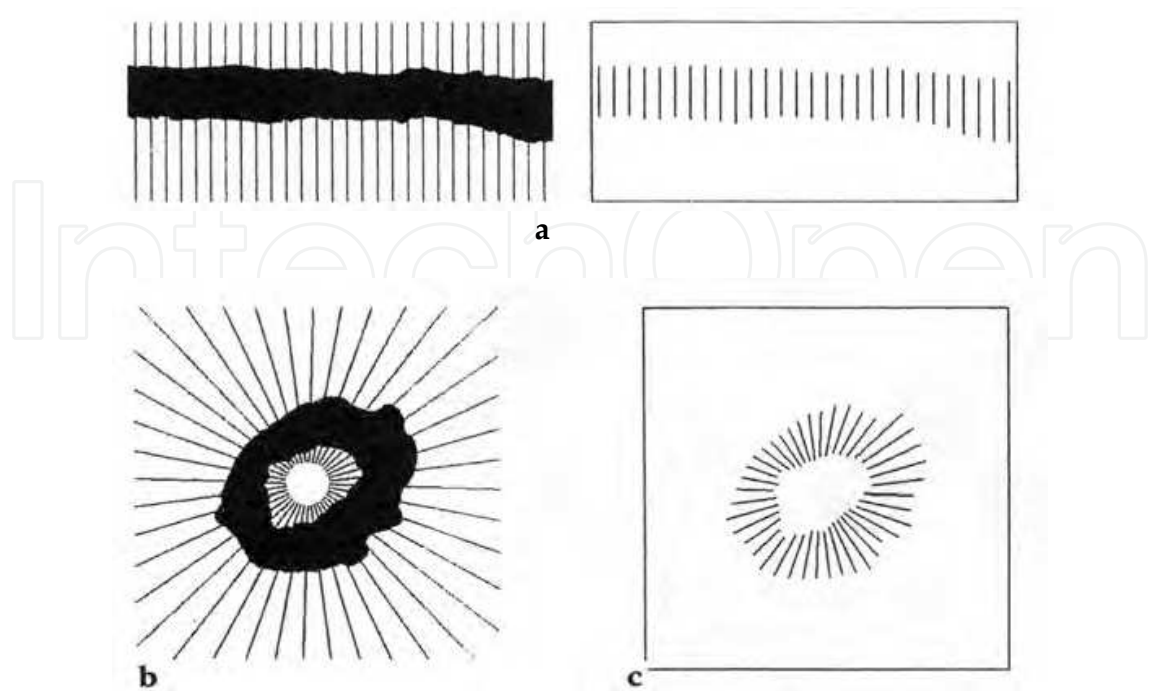
Fig. 16. Assessment of cluster parameters using logic operations.

Sometimes logic operations help to assess the characteristics of tracks (Russ, 2006). For instance, Fig. 16a shows how the alignment of two images – the initial cluster and a set of parallel lines – and the application of AND operation to them makes it possible to assess the width of the cluster and its profile. Another example (Fig. 16b) shows the application of AND operation to a cluster and a family of semistraight lines emanating from the centre of masses, for determining the profile of a convex cluster with a hole. PAVICOM's software package is provided with a block enabling similar operations.

a   b
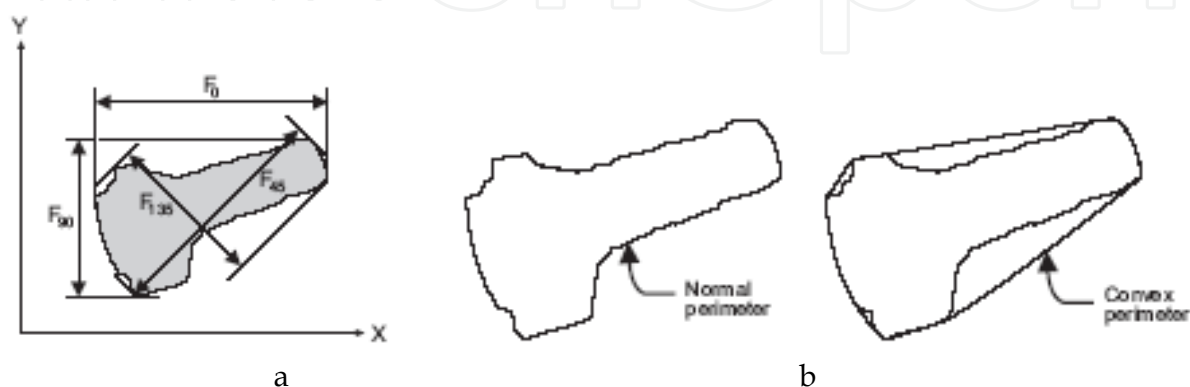
Fig. 17.

The shape of a cluster can also be assessed using Feret diameters – the distances between the outer tangents to the cluster drawn at a certain angle to the X axis. Figure 17a presents examples of Feret diameters F_0, F_{45}, F_{90} and F_{135}. Another important concept is the convex perimeter, which is a perimeter of such a convex figure, which is circumscribed around the cluster and has the least perimeter of all similar figures (Fig. 17b).

Tracks of nuclei in olivine have complex shapes. Etching of olivine in places of heavy nuclei passage forms channels shaped as "syringes" (see Fig. 18a). It should be noted that details of the geometric shape of a track can be important for the determination of the charge of a particle. For this reason, information on the pixels of the cluster boundary should be preserved during the clusterization. The result of clusterization in the case of a syringe-shaped cluster is given in Fig. 18b.

Proceeding from the physico-chemical pattern of interaction, the scheme of the formation of such an etchable channel can be described as follows. There is a threshold value of energy losses, D, to which E_{max} corresponds. For olivine, $D = 18$ MeV/(mg·cm^{-2}). If the energy of a particle is greater than E_{max}, no visible channel emerges after etching.

As it decreases, starting from E_{max}, when losses become greater than $D - 2$ MeV/(mg·cm^{-2}), the rate of etching begins to exceed the rate of etching of non-damaged sections and gradually rises until the value of losses $D + 2$ MeV /(mg·cm^{-2}) (energy E_1) is reached. A narrow etched channel (Fig. 20) emerges at this segment of the track. In the further deceleration of the particle ($E < E_1$) the etching rate sharply increases and, respectively, the etchable region of this segment acquires a larger diameter. At the end of the track before the particle is stopped the energy losses again drop down below the threshold D, and the channel ends with a narrow spike (Fig. 20).

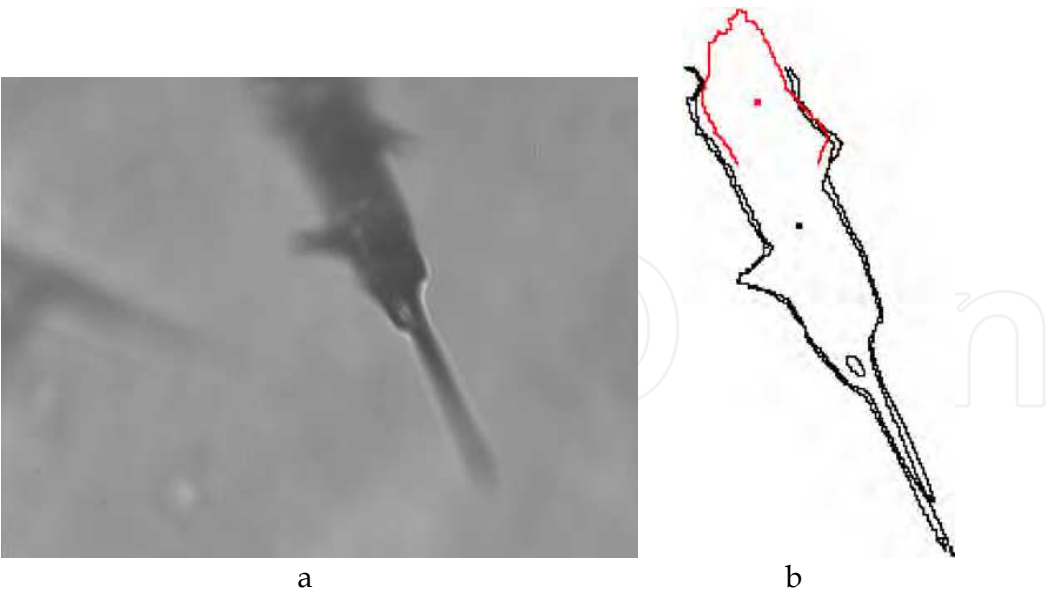a   b

Fig. 18. An example of a track of a galactic cosmic-ray heavy nucleus in olivine (a); the result of its recognition by the program (b). The track shown in Fig. 18a has an extension to the higher adjacent field of vision. In Fig. 18b, this extension is found by means of a special algorithm of searching for track extensions on adjacent fields of vision and is highlighted in red. It can be seen that the fields of vision are partially overlapped, which facilitates the alignment of adjacent fields of vision in the search for track extensions.

Thus, the etchable channels for heavy nuclei are shaped as "syringes". Figure 21 presents examples of images of real channels in olivine, which confirm the existence of the above described mechanism.
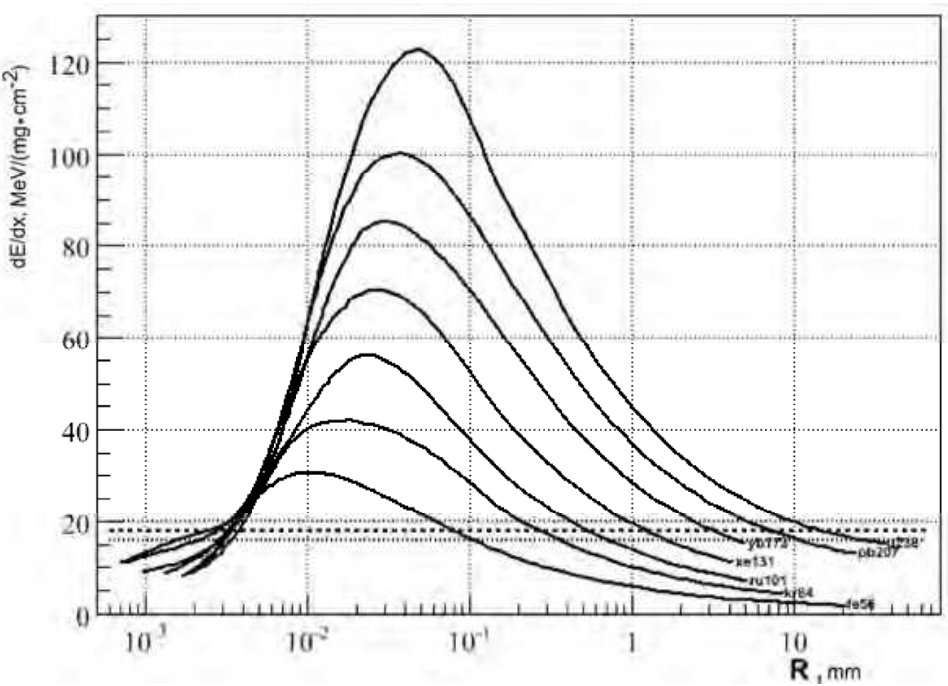
Fig. 19. Ionization losses of $_{26}^{56}$Fe, $_{36}^{84}$Kr, $_{44}^{101}$Ru, $_{54}^{131}$Xe, $_{70}^{173}$Yb, $_{82}^{207}$Pb, $_{92}^{238}$U nuclei in olivine depending on the residual run.
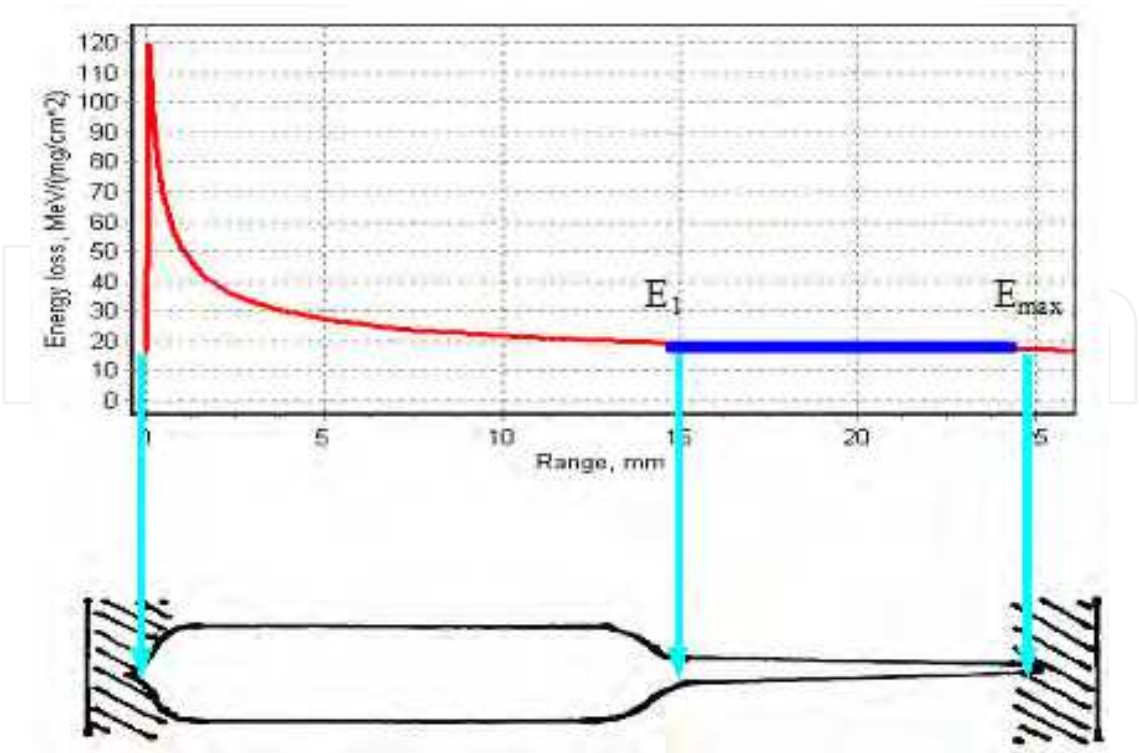
Fig. 20. A scheme of the formation of an etched section of a track in olivine. *Top*, the value of ionization losses. *Bottom*, shapes of various sections of the track.
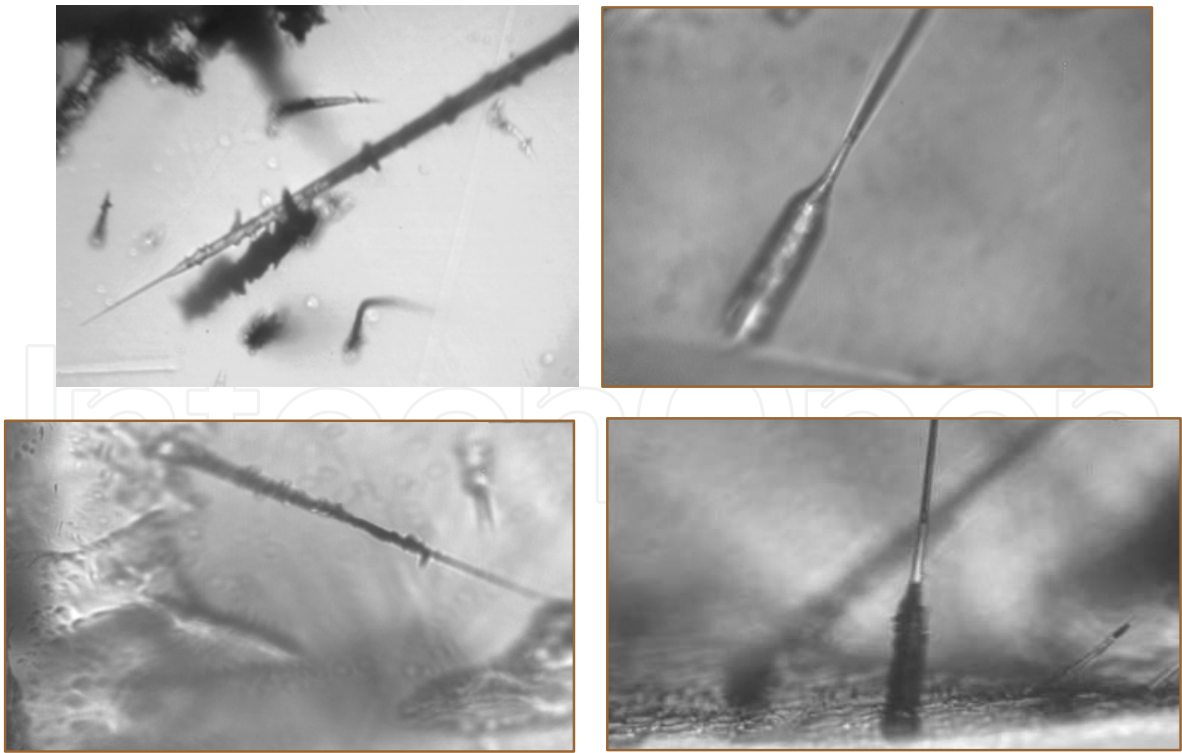

Fig. 21. Photographs of the tracks of nuclei in olivine.

As seen in Fig. 19, the length of the etchable channel can reach several millimetres or even more. At the same time, the size of most olivine crystals available for analysis is 2–3 mm.

This indicates that in the case of very heavy nuclei part of the etchable segment of a track proves to be outside the crystal.
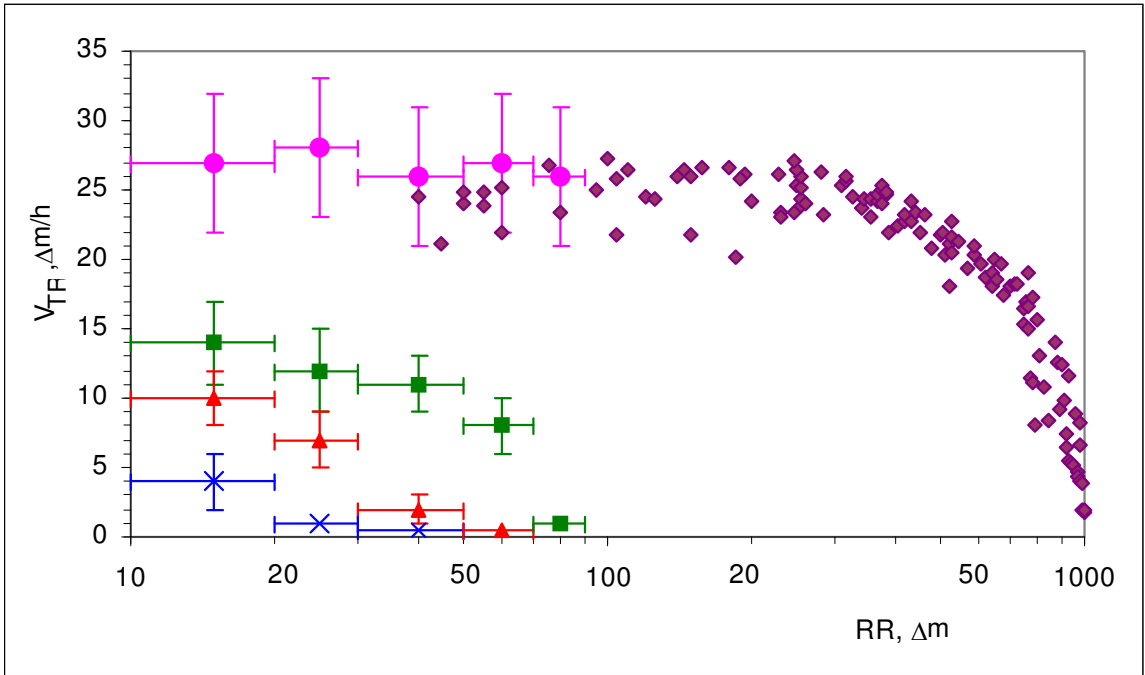
Fig. 22.

As it was already pointed out, the main aim of the project OLIMPIYA is to determine the charge composition of cosmic rays in the region of heavy and superheavy nuclei. The value of the charge is related to the characteristics of the etched track. The major of them is the etchable length L_{etch}, however, as we already mentioned, for very heavy nuclei it exceeds the sizes of olivine specimens and could not be found by available means. As a way out of the situation, it was proposed to use an additional value – the etching velocity. This value changes during the etching and increases as we approach the stoppage point of the particle (Perron & Bourot-Denise, 1986; Perron & Maury, 1986). Figure 22 shows the dependence of the etching velocity on charge and residual run *RR* (Perron & Bourot-Denise, 1986), i.e., practically before the stoppage point. (The PAVICOM facility processed the data of the calibration of olivines by the U, Xe, Kr, Au nuclei.)

In the general form, the dependence of the etching velocity *V* on charge *Z* and residual length *L* can be presented as a surface shown in Fig. 23, whose values for the missing charges are obtained by interpolation.

The method of assessing the value of charge consists in the two-dimensional interpolation of the surface (Fig. 23) by the measured values of *V* and *L* for a track etched in olivine.

Figure 24 shows the result of such a procedure for the heaviest nuclei. The family of the curves shown by coloured squares, represents the dependence of $Z(V, L)$. Blue circles with errors are the results of our measurements. The size of errors along the vertical and horizontal axes reflects the accuracy of the measurements. It is seen that the accuracy of charge determination depends on the position of points on the plane (*V*, *L*) and is from ±1 up to ±2.
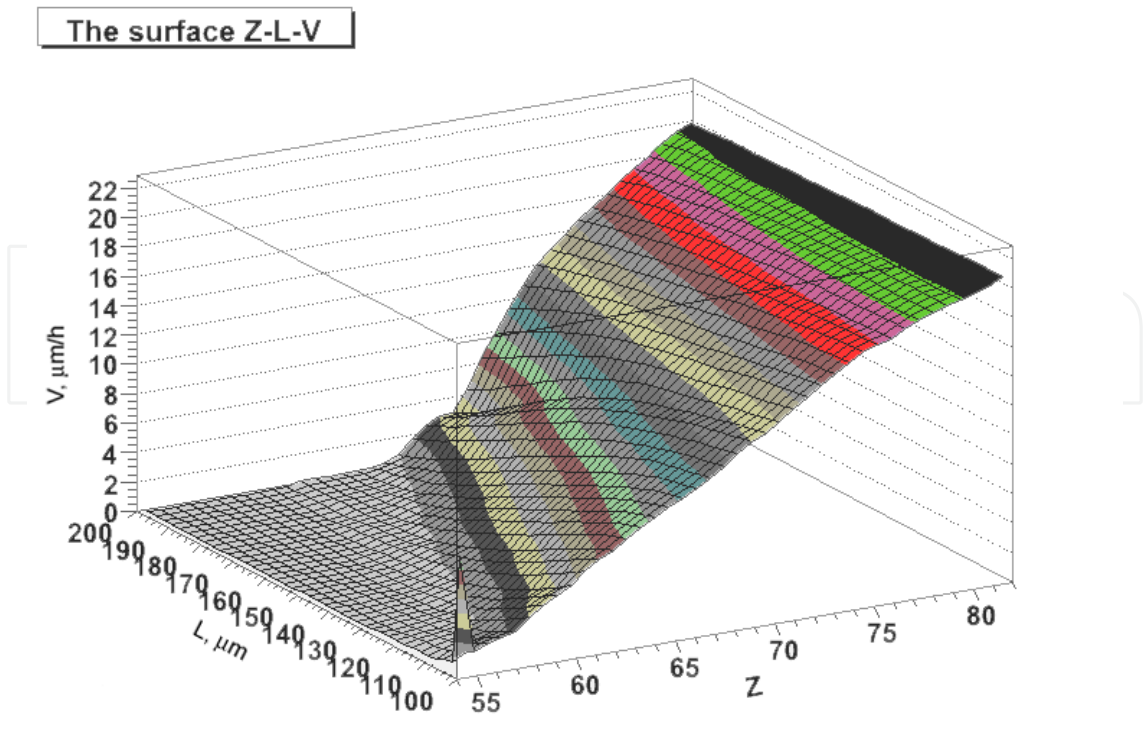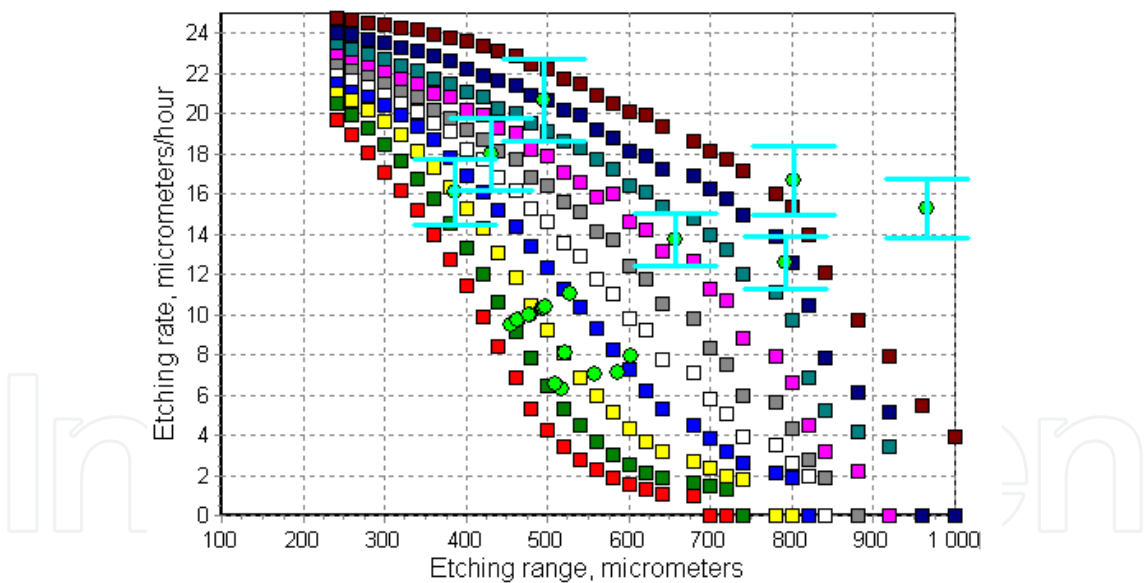
Fig. 23.

Fig. 24.

To date, 133 crystals from the Marjalahti meteorite and 37 from the Eagle Station meteorite have been processed; 4900 and 1839 tracks, respectively, have been found and identified. Of them, about 40 tracks have been assigned to nuclei with $Z \geq 88$. Among them, 5 events with $Z \geq 92$ have been found. The ratio of the abundance of nuclei with $Z \geq 88$ to that of nuclei with $74 \leq Z \leq 87$ is 0.045 ± 0.015 (Marjalahti) and 0.025 ± 0.02 (Eagle Station). These values are slightly larger than in the UHCRE experiment (0.0147 ± 0.0032) (Donnelly et al., 1999), but are well consistent with the data of the TREK, HEAO and Ariel experiments (Binns et

al., 1989; Fowler et al., 1987; Westphal et al., 1998). Figure 25 shows the charge distribution of tracks of nuclei we obtained in the course of the project OLIMPIYA, as compared with the abundance of galactic nuclei obtained in the HEAO and Ariel experiments (Binns et al., 1989; Fowler et al., 1987; Westphal et al., 1998).

Three superlong tracks (L_{tr} > 700 µm), whose etching speed was V_{etch} > 35 µm/h were found in the course of the project OLIMPIYA. If it is taken into account that the experimentally measured maximal etching rate of tracks in olivine for uranium nuclei before their stop is $V_{etch, U}$ = 26 ± 1 µm/h, then it becomes clear that the charges of these nuclei significantly exceed $Z = 92$. As in this region of charges the function $Z(RR, V_{etch})$ is unknown, the function $Z(RR \approx 50, V_{etch})$ at a residual range $RR \approx 50$ nuclei, for which the experimental data of the calibration measurements are available, was extrapolated to assess the charge of the transuranium nuclei in the first approximation. In this case, the lower boundary of the charge was assessed to be $Z = 105$ (Aleksandrov et al., 2011).

Thus, the data on the charge composition of approximately 600 nuclei with charge more than 55, whose distribution is in agreement with the data of other experiments, were obtained in the project OLIMPIYA. Besides, tracks of three superheavy nuclei of galactic cosmic rays were found and identified in the studied crystals of olivines from meteorites. In the first approximation, their charge is within the interval of $105 < Z < 130$. There is no doubt that the results obtained in the project OLIMPIYA confirm the hypothesis on the existence of "stability islands" for natural trans-Fermi nuclei.

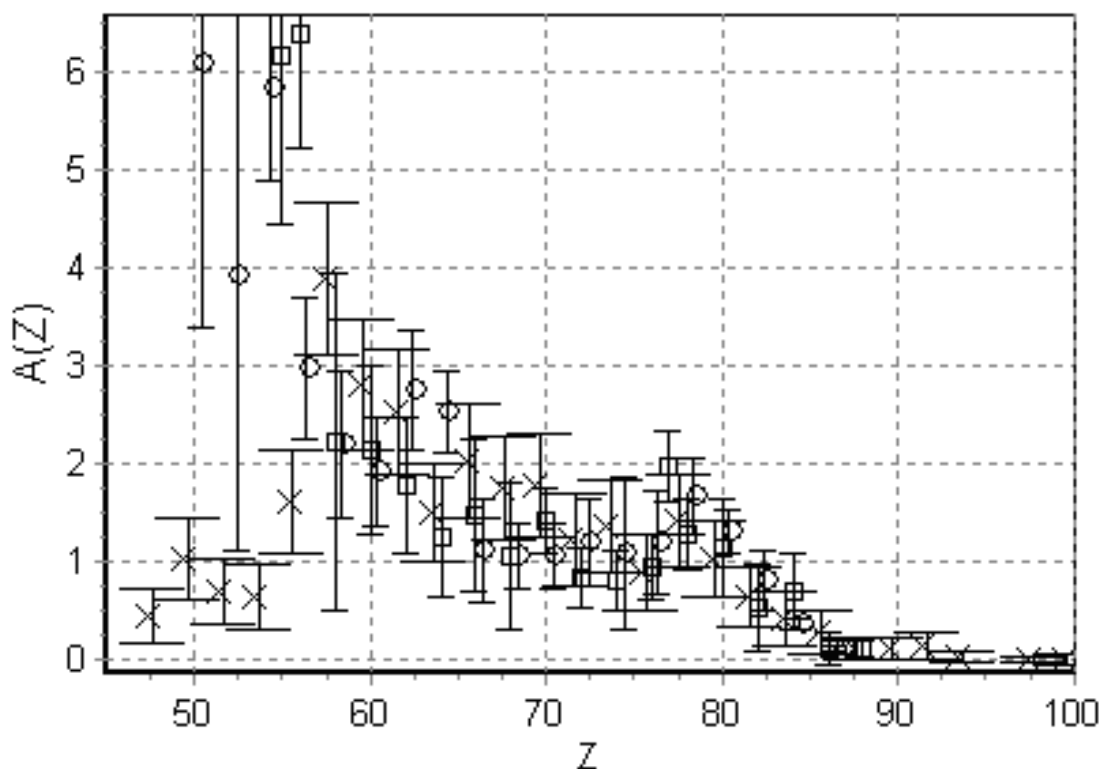Fig. 25. Abundance of superheavy nuclei $A(Z)$ ($A_{Fe} = 10^6$). Squares – HEAO (Binns et al., 1989; Fowler et al., 1987; Westphal et al., 1998), circles – Ariel (Binns et al., 1989; Fowler et al., 1987; Westphal et al., 1998), crosses – own results.

6. Conclusions

Thus, the worked out image recognition methods were successfully used in processing the data of various track detectors. An important advantage of the developed software package for the PAVICOM facility is its universal character, which makes it possible to combine separate components into a user program without any significant modifications and corrections. At present, work is underway to elaborate the prospects of using PAVICOM and accumulated experience of automated recognition of images for studies of neutrinoless double beta decay, research into the inner structure of industrial objects by means of muon radiography, expansion of the PAVICOM potential for recognition of objects on images in various innovation works, e.g., in automation of blood parameters in medicine.

7. References

Acquafredda, R. et al. (2009). The OPERA Experiment in the CERN to Gran Sasso Neutrino, *JINST* P04018, Vol. 4, April.

Aleksandrov, A.B.; Apacheva, I.Yu.; Goncharova, L.A.; Konovalova, N.S.; Orlova, G.I.; Polukhina, N.G.; Starkov, N.I.; Feinberg, E.L. & Chernyavsky, M.M. (2005a). The Method of Measuring Charges of Relativistic Nuclei in Nuclear Emulsion on the Automated Facility PAVICOM, LPI Preprint No. 29 (in Russian).

Aleksandrov, A.B.; Apacheva, I.Yu.; Goncharova, L.A.; Merzon, G.I.; Polukhina, N.G.; Starkov, N.I.; Feinberg, E.L. (2005b). The Method of Automated Processing the Data of Emulsion Trackers for Studies of Pb–Pb Interactions at the Energy of 158 GeV/nucleon, LPI Preprint No. 23 (in Russian).

Aleksandrov, A.; Polukhina, N. & Starkov, N. (2006). The Pattern Recognition Software for Automatic Treatment of Track Detector Data at the PAVICOM Completely Automated Measuring Facility, *23rd International Conference on Nuclear Tracks in Solids*; Program&Abstracts; p. 84; Beijing, China, September 11-15, 2006.

Aleksandrov, A.B.; Goncharova, L.A.; Davydov, D.A.; Feinberg, E.L.; Polukhina, N.G.; Publichenko, P.A. & Roganova, T.M. (2007a). Automated Methods of Processing Track Detectors Based on the PAVICOM Facility, Pis'ma v *Fiz. Elementarn. Chastits i Atomn. Yadra*, Vol. 4, No. 1 (137), pp. 170–175 (in Russian).

Aleksandrov, A.B.; Goncharova, L.A.; Konovalova, N.S.; Orlova, G.I.; Peresad'ko, N.G.; Polukhina, N.G.; Starkov, N.I.; Tarasova, I.Yu.; Chernyavsky, M.M. & Shchelkanov, A.O. (2007b) The Method of Measuring Charges of Relativistic Nuclei in Nuclear Emulsion at the Automated Facility PAVICOM, *Pribory I Tekhnika Eksperimenta*, Vol. 50, No. 4, p. 469 (in Russian).

Aleksandrov, A.B.; Vladymyrov, M.S.; Goncharova, L.A.; Konovalova, N.S.; Orlova, G.I.; Polukhina, N.G.; Starkov, N.I.; Chernyavsky, M.M. & Shchelkanov, A.O. (2007c) Automation of Measurements in Thick-Layer Nuclear Emulsions in Longitudinal Irradiation by Nuclei with Energy of 1 GeV per Nucleon with the View to Obtain Survey Information on Charge States of Secondary Particles, LPI Preprint No. 4 (in Russian).

Aleksandrov, A.B. (2009). *PhD Thesis*, Lebedev Physical Institute, Moscow (in Russian).

Aleksandrov, A.B.; Bagulya, A.V.; Vladymyrov, M.S.; … Polukhina, N.G. et al. (2010). Charge Spectrum of the Nuclei of Galactic Cosmic Rays in Olivines from Meteorites, *Uspekhi Fiz. Nauk*, Vol. 180, No. 8, pp. 839–842 (in Russian).

Aleksandrov, A.B.; Bagulya, A.V.; Vladimirov, M.S. et al. (2011). Results of Investigations Associated with the Search for Tracks of Relict Galaxy Nuclei in Olivine Crystals from Meteorites. *Proceedings of 32nd International Cosmic Ray Conference*, Beijing, 2011, in print.

Alexandrov, A.; Kashkarov, L.; Polukhina, N. & Starkov, N. (2008). The Pattern Recognition Software for Automatic Treatment of Track Detector Data at the PAVICOM Completely Automated Measuring Facility, *Radiation Measurements*, Vol. 43, Suppl. 1, August 2008, Pages S120-S124 Proceedings of the 23rd Int. Conference on Nuclear Tracks in Solids.

Astafyeva, N.M.; … Feinberg, E.L.; Polukhina, N.G. et al. (1997). Peculiarities of Secondary Particle Generation Process in Pb–Pb Interactions at 158 A GeV, *6th Conference on the Intersections of Particle and Nuclear Physics*, pp. 269-273.

Belovitsky, G.E.; Konobeevsky, E.S.; Zavrazina, V.P.; Zuev, S.V.; Polukhina, N.G.; Starkov, N.I.; Aleksandrov, A.B.; Lukyanov, S.M. & Sobolev, Yu.G. (2006). Discrimination of the trajectories of charged particles in nuclear emulsions. *Izvestiya RAN*, Vol. 70, No. 5, pp. 646–649 (in Russian).

Benton, E.V.; Curtin, S.B.; Raju, M.R. & Tobias, C.A. (1970) Studies of Negative Pion Beams by Means of Plastic Nuclear Track Detectors. In: *Proc. 7th Int. Colloq. Corpuscular Photography and Visual Solid Detectors,* Barselona, pp. 423–428.

Binns, E.V. et al. (1989). *ApJ*, Vol. 346, p. 997.

Birot, A.; Adroguer, B. & Fontan, J. (1970) Vertical Distribution of Radon 222 in the Atmosphere and its Use for Study of Exchange in the Lower Troposphere, *J. Geophysics Res.,* Vol. 75, pp. 2373–2383.

Bisnovatyi-Kogan, G.S. & Chechetkin, V.M. (1979). *Uspekhi Fiz. Nauk*, Vol. 127, p. 263 (in Russian).

Bock, R.K. et al. (2000). *Data Analysis Techniques for High-energy Physics*, 2nd ed., Cambridge University Press.

Boos, E.G.; Feinberg, E.L.; … Polukhina, N.G. et al. (1996). Investigation of Central Pb–Pb Interactions at Energies of 160 GeV/Nucleon with the Help of the Emulsion Magnetic Chamber, *Experiments at CERN in 1996*, Geneva, ISSN 0259-093X, pp. 122–123.

Burger, G.; Frunauer, F. & Paretzke, H. (1970) The Applicability of Track Detectors in Neutron Dosimetry. In: *Proc. Symp. Adv. Rad. Detectors*. International Atomic Energy Agency, Vienna, paper Sm-143.17.

Chan, J.H. & Price, P.B. (1975) Composition and Energy Spectra of Heavy Nuclei of Unknown Origin Detected on Skylab, *Phys. Rev. Lett.*, Vol. 35, pp. 539–542.

Chernavskaya, O.D. et al. (1996). The Central Pb–Pb Interactions with Energies 158 GeV/nucleon, *Proc. of the 28th International Conference on High Energy Physics*, Warsaw, Vol. 1, pp. 941–942.

Dobrotin, N.A. et al. (1999). Studies of Central Pb–Pb Interactions at High Energies, *Izvestiya AN, Ser. Phys.*, Vol. 63, No. 3, pp. 485–488 (in Russian).

Donnelly, J. et al. (1999). Proc. of the 26th Int. Cosmic Ray Conf., OG1.1.30.

Dremin, I.M. (2006). Ring-like Events: Cherenkov Gluons or Mach Waves? *Nucl. Phys. A*; hep-ph/0507167.

Dremin, I.M.; Ivanov, O.V.; Kalinin, S.A; …. Polukhina, N.G. et al. (2000). Wavelet Patterns in Nucleus–Nucleus Collisions at 158 A GeV, *Proc. of the 4th Rencontres du Vietnam*, pp. 531–533.

Dremin, I.M.; Ivanov, O.V.; Kalinin, S.A.; Kotelnikov, K.A.; Nechitailo, V.A. & Polukhina, N.G. (2001a). Wavelet-Patterns in Nucleus–Nucleus Collisions at 158 A GeV, *Phys. Lett. B*, Vol. 499, No. 1–2, pp. 97–103, hep-ph/0007060.

Dremin, I.M.; Ivanov, O.V.; Kalinin, S.A; …. Polukhina, N.G. et al. (2001b). Wavelet Patterns in Nucleus–Nucleus Collisions at 158 A GeV, *Phys. Lett. B*, Vol. 499, No. 1–2, pp. 97–103.

Eskut, E. et al. (2008). Final Results from a Search for Nu-Mu to Nu-Tau Oscillations with the CHORUS Experiment, Publ. Ref.: CERN-PH-EP/2007-034, arXiv:0710. 3361, *Nucl. Phys. B*, Vol. 793, pp. 326–343.

Feinberg, E.L.; Polukhina, N.G. & Kotelnikov, K.A. (2004). The Completely Automated Measuring Facility PAVICOM for Processing Experimental Material of Track Detectors, *Fizika Elementarnykh Chastits i Atomnogo Yadra*, Vol. 35, No. 3, pp. 763–787 (in Russian).

Fowler, F.H. & Perkins, D.H. (1961) The Possibility of Therapeutic Applications of Beams of Negative π Mesons, *Nature*, Vol. 189, pp. 524–528.

Fowler, P.H.; Adams, R.V.; Cowen, V.G. & Kidd, J.M. (1970) The Charge Spectrum of Very Heavy Cosmic Ray Nuclei, *Proc. Roy. Soc. Lond.*, A318, 1–43.

Fowler, P.H. et al. (1987). *ApJ*, Vol. 314, p. 739.

Frank, A.L. & Benton, E.V. (1975) Active and Passive Radon–Daughter Dosimeters Using Track-Etch Detectors. Dept. of Physics, Univ. of San Francisco, Tech. Report 39.

Fremlin, J.H. & Abu-Jarad, F. (1980) Alpha Emitters in the Environment. I: Natural Sources, *Nucl. Instr. Meth.*, Vol. 173, pp. 197–200.

Ginzburg, V.L. (1999). Which Problems of Physics and Astrophysics Appear Today the Most Important and Interesting? *Uspekhi Fiz. Nauk*, Vol. 169, p. 419 (in Russian).

Glaser, D.A. (1952) Some Effects of Ionizing Radiation on the Formation of Bubbles in Liquids, *Phys. Rev.*, Vol. 87, No. 4.

Kodama, K. et al. (2008). Detection and Analysis of Tau-Neutrino Interactions in DONUT Emulsion Target, *Nuclear Inst. And Meth. A*, Vol. 493 (202), pp. 45–66.

Kramarovsky, Ya.M. & Chechev, V.P. (1987). *Synthesis of Elements in the Universe*, Moscow, Nauka (in Russian).

Oganesyan, Yu.Ts. (2001). *Vestnik RAN*, Vol. 71, p. 590 (in Russian).

O'Sullivan, D.; Thompson, A.; Daly, J.; O'Ceallaigh, C. et al. (1980). A Solid State Track Detector Array for the Study of Ultraheavy Cosmic Ray Nuclei in Earth Orbit. In: *Proc. 10th Int. Conf. Solid State Nucl. Track Detectors*, Lyon, and Suppl. 2, Nucl. Tracks, Pergamon, Oxford, pp. 1011–1019.

Perron, C. & Bourot-Denise, M. (1986). Heavy Ion Track Etch Rate Measurements and Track Structure in a Mineral, *Int. J. Radiat. Appl. Instrum., D Nuclear Track*, Vol. 12, No. 1–6, p. 29.

Perron, C. & Maury, M. (1986). Very Heavy Ion Track Etching in Olivin, *Int. J. Radiat. Appl. Instrum., D Nuclear Track*, Vol. 11, No 1/2, p. 73.

Polukhina, N.G. (2006). *DSc Thesis*, Lebedev Physical Institute, Moscow (in Russian).

Pratt, U. (1982). *Digital Processing of Images, Vol. 2*, Mir, Moscow (in Russian).

Price, P.B.; Fleischer, R.L.; Peterson, D.D. et al. (1967). Identification of Isotopes of Energetic Particles with Dielectric Track Detectors, *Phys. Rev.,* Vol. 164, pp. 1618–1620.

Price, P.B.; Fleischer, R.L.; Peterson, D.D. et al. (1968). High Resolution Study of Low Energy Cosmic Rays with Lexan Track Detectors, *Phys. Rev. Lett.*, Vol. 21, pp. 630–633.

Russ, John C. (2006). The Image Processing Handbook, Fourth edition, CRC Press, London, New York.

Savvides, E.; Manolopoulou, M.; Papastefanou, C. & Charalambous, S. (1985). A Simple Device for Measuring Radon Exhalation from the Ground, *Int. J. Appl. Radiat. Isotop.* Vol. 36, pp. 79–81.

Starkov, N.I. (2010). DSc Thesis, Lebedev Physical Institute, Moscow (in Russian).

Strutinsky, V.M. (1967). *Nucl. Phys.*, Vol. A95, p. 420.

Vladymyrov, M.S.; Aleksandrov, A.B.; Chernyavsky, M.M.; Goncharova, L.A.; Orlova, G.I.; Polukhina, N.G.; Starkov, N.I.; Tsarev, V.A.; Galkin, V.I.; Publichenko, P.A.; Roganova, T.M. & Sazhina, G.P. (2008). PAVICOM Facility for Treatment of OPERA Experimental Data, *Proceedings of Science*, Nufact08, p. 143, Valencia, June 2008 http://pos.sissa.it/archive/conferences/074/143/Nufact08_143.pdf.

Westphal, A.J. et al. (1998). *Nature*, Vol. 396, p. 50.

Wilson, C.T.R. (1897). *Phil. Trans.,* Vol. 189, p. 265.

Zeldovich, Ya.B. (1960). *Zhurnal Eksp. Teor. Fiziki*, Vol. 38, p. 1123 (in Russian).
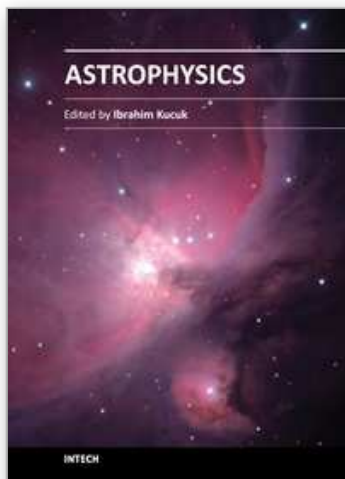
Astrophysics

Edited by Prof. Ibrahim Kucuk

This book provides readers with a clear progress to theoretical and observational astrophysics. It is not surprising that astrophysics is continually growing because very sophisticated telescopes are being developed and they bring the universe closer and make it accessible. Astrophysics Book presents a unique opportunity for readers to demonstrate processes do occur in Nature. The unique feature of this book is to cover different aspects in astrophysics covering the topics: • Astronomy • Theoretical Astrophysics • Observational Astrophysics • Cosmology • The Solar System • Stars • Planets • Galaxies • Observation • Spectroscopy • Dark Matter • Neutron Stars • High Energy Astrophysics

How to reference

In order to correctly reference this scholarly work, feel free to copy and paste the following:

A.B. Aleksandrov, N.G. Polukhina and N.I. Starkov (2012). Methods for Image Recognition of Charged Particle Tracks in Track Detector Data Automated Processing, Astrophysics, Prof. Ibrahim Kucuk (Ed.), ISBN: 978-953-51-0473-5, InTech, Available from: http://www.intechopen.com/books/astrophysics/methods-for-image-recognition-of-charged-particle-tracks-in-track-detector-data-automated-processing

INTECH
open science | open minds